Polarizable Atomic Multipole Water Model for Molecular Mechanics Simulation

Pengyu Ren and Jay W. Ponder*

Department of Biochemistry and Molecular Biophysics, Washington University School of Medicine, St. Louis, Missouri 63110

Received: December 23, 2002; In Final Form: March 19, 2003

A new classical empirical potential is proposed for water. The model uses a polarizable atomic multipole description of electrostatic interactions. Multipoles through the quadrupole are assigned to each atomic center based on a distributed multipole analysis (DMA) derived from large basis set molecular orbital calculations on the water monomer. Polarization is treated via self-consistent induced atomic dipoles. A modified version of Thole's interaction model is used to damp induction at short range. Repulsion−dispersion (vdW) effects are computed from a buffered 14−7 potential. In a departure from most current water potentials, we find that significant vdW parameters are necessary on hydrogen as well as oxygen. The new potential is fully flexible and has been tested versus a variety of experimental data and quantum calculations for small clusters, liquid water, and ice. Overall, excellent agreement with experimental and high level ab initio results is obtained for numerous properties, including cluster structures and energetics and bulk thermodynamic and structural measures. The parametrization scheme described here is easily extended to other molecular systems, and the resulting water potential should provide a useful explicit solvent model for organic solutes and biopolymer modeling.

Introduction

Empirical potential energy functions derived from classical molecular mechanics are central to computational modeling at the atomic level. Molecular mechanics has long enjoyed great success in application to many classes of isolated, gas-phase organic compounds.[1] Beginning with the pioneering work of Bernal and Fowler,[2] water has probably been the target of more potential energy models than any other substance. An interesting overview and historical perspective on the development of water models was recently presented by Finney.[3]

Simple nonpolarizable pairwise-additive models that describe the average structure and energetics of liquid water have been in wide use for many years (e.g., TIP3P[4] and SPC[5]). The recently developed TIP5P potential exhibits excellent agreement with the experimental internal energy, density, and O···O radial distribution at room temperature.[6] These models typically use fixed atom-based partial charges to model electrostatics and include polarization response to the environment only in an averaged, mean-field sense. As a result, nonpolarizable potentials that provide excellent descriptions of the homogeneous bulk phase are poor models for gas phase clusters and for nonpolar solutes in polar solvents. For example, the gas phase binding energy of the water dimer is overestimated by more than 30% in the TIP5P model. In application to large biomolecular systems, there is concern that such models cannot correctly account for situations where the same nonpolarizable moiety is exposed to different electrostatic environments, either within a single large static structure or during a course of simulation. In addition, there is an inherent inconsistency in most nonpolarizable models related to their static inclusion of average bulk polarization within the potential. This results in internal energies and other properties that are derived against a gas-phase reference state that is already "pre-polarized" for the liquid phase. Although it is possible to correct for the resulting self-energy of the reference state, as in the SPC/E water model,[7] such corrections are not routinely used for heterogeneous systems.

In response to the above concerns, much effort has been expended on inclusion of explicit polarization within the next generation of empirical potentials.[8,9] Water has been the focus of many such studies due to its highly polarizable, hydrogen bonded nature, and obvious biological importance.

Partial atomic charge electrostatic models often lack sufficient mathematical flexibility to describe the electrostatic potential around molecules to within chemical accuracy. Williams[10] showed that optimal least-squares fits of atom-centered partial charges resulted in relative rms errors of 3−10% over a set of grid points in a shell outside the surface of a series of small polar molecules. These errors were reduced by 2−3 orders of magnitude via use of atomic multipoles through the quadrupole at each atomic center. For example, simple partial charge models for water are inherently unable to adequately describe the molecular dipole and quadrupole of the water monomer at the same time without resorting to extra charge sites.

Many-body polarization effects in water have large structural and energetic consequences that vary greatly with environment. Several methods are available to explicitly model the physics of polarization. The use of polarizable point dipoles is a classical approach with a long history in molecular simulation.[11] For water, a single-point dipole site can be placed either on the oxygen atom or near the center of mass. Alternatively, a more flexible model places induced dipoles on each atom, necessitating a distribution of polarizability among the three sites. This latter scheme has been adopted for our current model. Charge equilibration (Qeq) methods[12] compute absolute partial atomic charges that depend on the local environment and are a self-consistent result of achieving electronegativity equalization. The

* To whom correspondence should be addressed. Phone: (314) 362-4195. Fax: (314) 362-7183. E-mail: ponder@dasher.wustl.edu.

10.1021/jp027815+ CCC: $25.00 © 2003 American Chemical Society
Published on Web 05/24/2003

fluctuating charge (FQ) scheme is essentially a perturbation version of Qeq that dynamically modifies an initial partial charge distribution based on the same principle via an extended Lagrangian formulation.[13] Hybrid potentials that utilize both FQ and induced dipole polarization have been described.[14] Another recently proposed scheme attempts to account for penetration effects and polarization with a formally pairwise model based on screening of diffuse charges at close range.[15]

Previous attempts to parametrize a polarizable water model applicable across multiple phases date back to the "polarizable electropole" model of Barnes et al.[16] that treated electrostatics via a single site carrying the experimental dipole and quadrupole moments and isotropic dipole polarizability. An interesting polarizable and dissociable potential was suggested by Stillinger and David and applied to water clusters and ion monohydrates.[17] The original MCY model,[18] based on a fit to points on an ab initio dimer surface, has evolved into the NCC-vib potential[19] which includes induced dipole polarization and vibrational flexibility. Sprik and Klein[20] made an early attempt to modify the existing TIP4P potential to include polarization within a Drude oscillator framework particularly suitable for molecular dynamics simulation. The POL3 model[21] uses atomic polarizabilities taken from the undamped dipole interaction method due to Applequist.[22,23] POL3 water is not polarizable enough due to the exclusion of the intramolecular polarization. This is evidenced by its very low dimer binding energy of −5.45 kcal/mol and its use of atomic partial charges intermediate between nonpolarizable and more recent polarizable models. Another early water model from the Levy group[24] uses partial charges and induced dipoles on each atomic center, along with a Thole polarization damping scheme related to that used in the present work. Their use of only partial charges for the underlying permanent electrostatics results in a shallow flap angle for the dimer structure. Also, the Levy model is reported to have an insufficiently low liquid binding energy, which correlates with their overestimate of the self-diffusion constant. The early 4-site Dang−Chang model[25] has a single polarizable center placed along the H−O−H bisector. It yields generally reasonable results, but its dimer binding energy and liquid internal energy are not low enough, possibly due to the effort to enhance the liquid dynamics. The Thole-type model (TTM) of Burnham and Xantheas[26] was the other early model to apply the short-range polarization damping of Thole to water. The family of second generation of TTM models, TTM2-R[27] and TTM2-F,[28] exhibit improved properties and are further discused below.

A common feature of many recently developed water models is the use of high quality ab initio data as the basis for the electrostatic parameters. The early work of Buckingham and Fowler[29] used ab-initio-derived multipoles to model the directionality of van der Waals complex geometries. Dykstra was one of the first to systematically use higher-order polarizable multipole electrostatics within a traditional molecular mechanics formalism.[30,31] His MMC water model showed the promise of these techniques in predicting water cluster properties.[32] The NEMO models represent an attempt to bridge the gap between quantum chemistry and empirical potentials[33] with a water model based on rigorous decomposition of Hartree−Fock results.[34] Recently, a NEMO potential for formamide has been extended to encompass a Thole-style polarization model.[35] The MCDHO potential uses a harmonic oscillator potential to bind a mobile charge site to the oxygen position.[36] The MCDHO model appears to give a good representation of the dimer minimum and surface, as corroborated by its agreement with experimental second virial coefficient data. The ASP−W4 model[37] uses an elaborate dispersion formulation and one-site polarizabilities up to quadrupole−quadrupole. ASP−W4 and the related VRT(ASP−W) potential[38] have been applied to dimer and cluster properties, but bulk phase simulations have not been reported. Finally, the recently introduced POL5/TZ and POL5/QZ water models,[14] which combine fluctuating charge and induced dipole polarization, are compared to our new model.

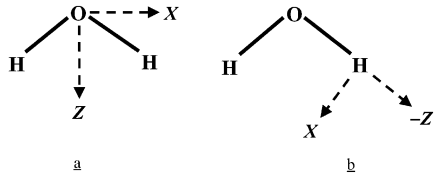

Figure 1. Local coordinate frame definitions. (a) For multipoles centered on oxygen, the H−O−H bisector is taken as the *Z* axis. The *X* axis is chosen to lie in the plane of the molecule and perpendicular to the *Z* axis. The *Y* axis is normal to the molecular plane and is chosen to yield a right-handed local coordinate system. (b) For hydrogen, the *Z* axis lies along the O−H bond, the *X* axis is in the molecular plane with its positive direction toward the second hydrogen, and the *Y* axis is chosen to give an orthogonal right-handed coordinate frame.

As a first step in the development of a set of general polarizable atomic multipole potentials (AMOEBA, atomic multipole optimized energetics for biomolecular applications) for modeling of organic and biomacromolecular systems, a new water potential is introduced. The AMOEBA water model is developed in such a way that it is applicable to water in various environments. Importantly, the water parameters are consistent with periodic table trends and with values we have derived for an extensive series of small organic molecules. Such consistency is a critical consideration if the water model is to be used in heterogeneous simulations.

Methods

Atomic Multipoles. Permanent atomic monopole, dipole, and quadrupole moments are placed on each atomic center. The components at each site can be written in polytensor form as $M = [q,\mu_1,\mu_2,\mu_3,Q_{11},Q_{12},...,Q_{33}]^T$. The dipole and quadrupole components require construction of a local coordinate frame at each site as illustrated in Figure 1 for the O and H atoms of water. For energy evaluations, the locally defined multipole moments are rotated into the global frame. It should be noted that the AMOEBA model uses traceless quadrupoles. It is not possible to uniquely convert traceless quadrupoles to the corresponding traced form. However, as pointed out by Stone,[39] after multiplication by a factor of $^1/_3$, traceless quadrupoles can be used directly in formulas based on the traced form. Because of the presence of local coordinate frames and aniostropic moments, both force and torque are generated at each multipole site. To facilitate Cartesian energy minimization and dynamics simulation, torques are converted into forces between the interacting multipole sites and the sites defining the corresponding local frames.

Polarization. Polarization effects are explicitly treated in the AMOEBA force field via mutual induction of dipoles at atomic centers. Atomic dipole polarizabilities can be derived from an empirical fit to experimentally known molecular polarizabilities. Values of such atomic dipole polarizabilities are coupled to the corresponding physical model applied during the fitting procedure, of which two types have been reported in the literature: additive[40,41] and nonadditive models.[22,42,43] In an additive model, polarization is ignored between atoms within the same molecule, and the sum of atomic polarizabilities therefore equals the total molecular polarizability. In general, additive models require

anisotropic atomic polarizabilities to accurately reproduce molecular polarizability tensors.

In a nonadditive model, mutual polarization exists among all polarizable sites, even those belonging to the same molecule. To avoid a "polarization catastrophe" at very short range, Thole[42] introduced a modification scheme in which dipole interactions are damped as though one of the point dipoles in each pairwise interaction is replaced by a smeared charge distribution. As a result, the dipole interaction energy approaches a finite value instead of becoming infinite as the separation distance approaches zero. A number of charge distribution models were tested,[42,43] and for each of the models, a single transferable isotropic polarizability for each chemical element was derived by fitting to experimental polarizabilities of a set of molecules. The results indicated that a variety of different damping models behaved rather similarly in terms of reproduction of molecular polarizabilities. The charge distribution adopted by the AMOEBA force field has the form

$$\rho = \frac{3a}{4\pi}\exp(-au^3) \tag{1}$$

where $u = R_{ij}/(\alpha_i\alpha_j)^{1/6}$ is the effective distance as a function of atomic polarizabilities of sites i (α_i) and j (α_j). The factor a is a dimensionless width parameter of the smeared charge distribution and controls the strength of damping.

Following Stone's notation,[39] multipole interaction T matrix elements, with $4\pi\epsilon_0$ omitted for clarity, are expressed as

$$T = \frac{1}{R}$$

$$T_\alpha = \nabla_\alpha T = -\frac{R_\alpha}{R^3}$$

$$T_{\alpha\beta} = \nabla_\alpha T_\beta$$

$$T_{\alpha\beta\gamma} = \nabla_\alpha T_\beta\gamma$$

$$\cdots\cdots$$

$$(\alpha,\beta,\gamma,\ldots = 1,2,3) \tag{2}$$

Using the charge distribution given by eq 1, the damped T matrix can be derived. It has been shown that the damped first-order T element is[42]

$$T_\alpha^{\mathrm{D}} = -[1-\exp(-au^3)]\frac{R_\alpha}{R^3} \tag{3}$$

The modified higher-order T matrix elements can be obtained successively by taking the derivative of the preceding lower rank elements:

$$T_{\alpha\beta}^{\mathrm{D}} = \lambda_5\frac{3R_\alpha R_\beta}{R^5} - \lambda_3\frac{\delta_{\alpha\beta}}{R^3}$$

$$T_{\alpha\beta\gamma}^{\mathrm{D}} = -\lambda_7\frac{15R_\alpha R_\beta R_\gamma}{R^7} + \lambda_5\frac{3(R_\alpha\delta_{\beta\gamma} + R_\beta\delta_{\alpha\gamma} + R_\gamma\delta_{\alpha\beta})}{R^5}$$

$$T_{\alpha\beta\gamma\eta}^{\mathrm{D}} = \lambda_9\frac{105R_\alpha R_\beta R_\gamma R_\eta}{R^9} - \lambda_7\frac{15(R_\alpha R_\beta\delta_{\gamma\eta} + R_\alpha R_\gamma\delta_{\beta\eta} + R_a R_\eta\delta_{\beta\gamma} + R_\beta R_\gamma\delta_{\alpha\eta} + R_\beta R_\eta\delta_{\alpha\gamma} + R_\gamma R_\eta\delta_{\alpha\beta})}{R^7} + \lambda_5\frac{3(\delta_\alpha\beta\delta_{\gamma\eta} + \delta_\alpha\gamma\delta_{\beta\eta} + \delta_{\alpha\eta}\delta_{\beta\gamma})}{R^5} \tag{4}$$

where the λ_i for $i \in \{3,5,7,9\}$ are the damping coefficients that modify the standard interactions

$$\lambda_3 = 1 - \exp(-au^3)$$

$$\lambda_5 = 1 - (1+au^3)\exp(-au^3)$$

$$\lambda_7 = 1 - \left(1 + au^3 + \frac{3}{5}a^2u^6\right)\exp(-au^3) \tag{5}$$

$$\lambda_9 = 1 - [1 + au^3 + (18a^2u^6 + 9a^3u^9)/35]\exp(-au^3)$$

After replacing the standard interaction matrix elements with the above damped ones, the energy, force, and electric field are computed in the usual fashion. In our AMOEBA model, only those interactions that involve induced dipoles are damped, while the interactions between permanent multipoles are not affected.

Induced Dipoles. The induced dipole at each atomic site is computed as $\mu_{i,\alpha}^{\mathrm{ind}} = \alpha_i E_{i,\alpha}$ where α_i is the atomic polarizability and $E_{i,\alpha}$ is the sum of the fields generated by both permanent multipoles and induced dipoles

$$\mu_{i,\alpha}^{\mathrm{ind}} = \alpha_i\left(\sum_{\{j\}} T_\alpha^{ij} M_j + \sum_{\{j'\}} T_{\alpha\beta}^{ij'}\mu_{j',\beta}^{\mathrm{ind}}\right) \quad \text{for } \alpha,\beta = 1,2,3 \tag{6}$$

where $M_j = [q_j,\mu_{j,1},\mu_{j,2},\mu_{j,3},\ldots]^T$ contains the permanent multipole components and $T_\alpha^{ij} = [T_\alpha,T_{\alpha 1},T_{\alpha 2},T_{\alpha 3},\ldots]$ is the interaction matrix between site i and j introduced in the previous section. The Einstein convention implying a summation over repeated subscripts is used. The set $\{j\}$ consists of all atomic sites outside the molecule containing i. The set $\{j'\}$ includes all atomic sites other than i itself, which is an intrinsic requirement of Thole's model. It can be shown[44] that the solution of the above self-consistent equation can be written as

$$\mu_{i,\alpha}^{\mathrm{ind}}(n+1) = \mu_{i,\alpha}^{\mathrm{ind}}(n) + \alpha_i\sum_{\{j'\}} T_{\alpha\beta}^{ij'}\mu_{j',\beta}^{\mathrm{ind}}(n) \quad \text{for } n = 0,1,2,\ldots \tag{7}$$

where $\mu_{i,\alpha}^{\mathrm{ind}}(0) = \alpha_i\Sigma_{\{j\}}T_\alpha^{ij}M_j$ is the "direct" induced dipole on site i due to the electric field from permanent multipoles of other molecules, and $\alpha_i\,\Sigma_{\{j'\}}\,T_{\alpha\beta}^{ij'}\mu_{j',\beta}^{\mathrm{ind}}(n)$ is the "mutual" induced dipole further induced by induced dipoles on all the other sites. Convergence of the iterative mutual induced dipole calculation is enforced and accelerated via successive overrelaxation (SOR)[45] using a value of $\omega = 0.75$ in

$$\mu_{j,\alpha}^{\mathrm{ind}}(n+1) = (1-\omega)\mu_{j,\alpha}^{\mathrm{ind}}(n) + \omega[\mu_{j,\alpha}^{\mathrm{ind}}(n) + \alpha_i\sum_{\{j'\}} T_{\alpha\beta}^{ij'}\mu_{j',\beta}^{\mathrm{ind}}(n)] \tag{8}$$

Ewald Summation. Electrostatic interactions for periodic systems are treated using the Ewald summation technique. Smith derived Ewald summation formulas for the interaction of permanent point multipoles through the quadrupole moment,[46] and two groups have recently described an Ewald treatment of dipole polarization due to fixed point charges and dipoles.[47,48]

In physical terms, polarization is an inseparable and nonadditive part of the total electrostatic interaction. However, it is computationally convenient to group together all electrostatic terms involving induced dipoles, to reflect the effect of polarization. The remaining electrostatic terms represent the "permanent" interactions that one finds in a nonpolarizable potential. Another practical reason to separate polarization terms is that, unlike the permanent multipole interactions, the short-range polarization interactions (energy, field, force, etc.) in our model are damped as described earlier.

TABLE 1: Force Field Parameters (where Only Nonzero Multiple Components are Listed)

O-H bond	b_0 (Å)	K_b (kcal/Å^2/mol)	O multipoles	(a.u.)
	0.9572	529.6	Q	−0.51966
H−O−H angle	θ_0 (deg)	K_θ (kcal/deg^2/mol)	d_z	0.14279
	108.50	34.05	Q_{xx}	0.37928
Urey−Bradley	l_0 (Å)	K_l (kcal/Å^2/mol)	Q_{yy}	−0.41809
	1.5537	38.25	Q_{zz}	0.03881
			H multipoles	(a.u.)
van der Waals	R^0 (Å)	ϵ (kcal/mol)	Q	0.25983
O	3.405	0.110	d_x	−0.03859
H	2.655	0.0135	d_y	−0.05818
$H_{\text{reduction}}$	91%		Q_{xx}	−0.03673
polarizability	α (Å^3)		Q_{yy}	−0.10739
O	0.837		Q_{xz}	−0.00203
H	0.496		Q_{zz}	0.14412

Using notation similar to that adopted by Smith,[46] we have derived the corresponding Ewald formulas for the polarization-related electric field, energy, force, and virial tensor as given in the Appendix. The "polarization energy" is defined as the energy contribution due to polarization, i.e., the total electrostatic energy of the system minus the contribution due to interactions between permanent multipoles. Thus, the polarization energy already includes the positive self-energy required for the system to become polarized. Similar definitions are applied to describe the polarization force and torque.

Model Development

The AMOEBA water potential consists of anharmonic bond, anharmonic angle, and Urey−Bradley terms to describe the intramolecular geometry and vibrations, a buffered 14−7 vdW form to account for repulsion and dispersion interactions, plus an electrostatic model with permanent atomic multipoles (charge, dipole, and quadrupole) and isotropic atomic dipole polarizabilities. The complete set of parameters is listed in Table 1.

Valence Terms. Our model includes full intramolecular flexibility. It has been argued that flexible water models are not superior to their rigid counterparts because of the inherent quantum nature of stretching and bending vibrations.[49] However, intramolecular flexibility is clearly important in the modeling of larger molecules with additional conformational options. Thus, it seems consistent to retain the same intramolecular degrees of freedom in a solvent model to be used in solvating larger species. The functional forms for bond stretching and angle bending were taken from the MM3 force field[50] and include anharmonicity through the use of higher-order deviations from ideal bond lengths and angles

$$U_{\text{bond}} = K_b(b - b_0)^2[1 - 2.55(b - b_0) - 3.793125(b - b_0)^2] \quad (9)$$

$$U_{\text{angle}} = K_\theta(\theta - \theta_0)^2[1 - 0.014(\theta - \theta_0) + 5.6 \times 10^{-5}(\theta - \theta_0)^2 - 7.0 \times 10^{-7}(\theta - \theta_0)^3 + 2.2 \times 10^{-8}(\theta - \theta_0)^4] \quad (10)$$

An additional valence term was used to model the coupling between stretching and bending modes. A Urey−Bradley functional form was chosen over the MM3 stretch−bend term as it is better able to reproduce splitting of the symmetric and asymmetric stretch vibrations. The Urey−Bradley term consists of a simple harmonic function

$$U_{\text{UB}} = K_l(l - l_0)^2 \quad (11)$$

TABLE 2: Electrostatic Moments and Polarizability of the Gas-Phase Water Monomer[a]

	dipole	quadrupole			polarizability		
	d_z	Q_{xx}	Q_{yy}	Q_{zz}	α_{xx}	α_{yy}	α_{zz}
AMOEBA[b]	1.773	2.50	−2.17	−0.33	1.672	1.225	1.328
	(1.853)	(2.35)	(−2.16)	(−0.20)	(1.660)	(1.221)	(1.332)
POL5/TZ	1.854	2.34	−2.34	0.00	1.494	1.060	1.320
TTM/TTM2-R	1.853	2.51	−2.23	−0.28	1.615	1.294	1.370
Expt	1.855[c]	2.63[d]	−2.50[d]	−0.13[d]	1.528[e]	1.415[e]	1.468[e]
ab initio[f]	1.840	2.57	−2.42	−0.14	1.47	1.38	1.42

[a] Values for a coordinate system where z is the C_2 axis, the molecule lies in the xz plane, and the O atom is along the negative z axis. [b] AMOEBA values at the ideal bond angle of 108.5°. Values corresponding to the experimental bond angle of 104.52° are listed in parentheses. [c] Reference 77. [d] Reference 143. [e] Reference 144. [f] Reference 145.

TABLE 3: Water Dimer Equilibrium Properties: Dissociation Energy D_e (kcal/mol), O−O Distance r_{O-O} (Å), α and θ Angles (degree) as Defined in Figure 2, Average Dipole Moment Per Molecule $\langle\mu_{\text{mol}}\rangle$ (Debye), and Total Dipole Moment μ_{tot} (Debye)

	POL5/TZ	TTM2-R	TTM2-F	AMOEBA	ab initio	expt
D_e	4.96	4.98	5.02	4.96	4.98[a], 5.02[b]	5.44 ± 0.7[e]
r_{O-O}	2.896	2.894	2.899	2.892	2.907[a], 2.912[b]	2.976[f]
α	4.69			4.18	4.18[a], 5.5[b]	−1 ± 10[f]
θ	62.6			57.2	56.9[a], 55.6[b]	57 ± 10[f]
$\langle\mu_{\text{mol}}\rangle$	2.06			2.02	2.1[c]	
μ_{tot}	2.44			2.54	2.76[d]	2.643[f]

[a] Reference 93. Values taken from data in tables II, III, and VII, based on calculations at CCSD(T)/TZ2P(f,d)+dif corrected for BSSE. [b] Reference 92. Complete basis set estimate from correction of CCSD(T) calculations. [c] References 146. Derived from DMA calculation directly on water dimer minimum. [d] Reference 98. From MP2/TZ2P++ calculations. [e] Reference 147. Estimate after vibrational correction of experimental ΔH at 373 K. [f] Reference 148. Microwave spectra from molecular beam resonance experiments at 20 K.

where l is the distance between the two hydrogen atoms of a water molecule.

The ideal bond length, b_0, was set to the experimental value of 0.9572 Å.[51] The ideal bond angle, θ_0, was set to 108.5°, and a Urey−Bradley ideal distance of $l_0 = 1.5326$ Å was used. This angle is some 4° larger than the experimental gas-phase angle of 104.52° but smaller than the tetrahedral angle of 109.47° used by the SPC model[5] and other empirical potentials. The large ideal bond angle is necessary to produce the correct average angle in liquid water, as discussed below. The three force constants for the valence terms were fit to exactly reproduce the gas-phase vibrational frequencies of the water monomer at the experimental geometry.[52] These constants were not reoptimized even though we subsequently adopted a somewhat larger H−O−H ideal angle, which affects the gas-phase bending frequency only slightly (see Table 8).

Repulsion−Dispersion. The buffered 14−7 potential[53] has been applied to model pairwise additive vdW interactions. The functional form is

$$U_{ij}^{\text{Buff}} = \epsilon_{ij}\left(\frac{1+\delta}{\rho_{ij}+\delta}\right)^{n-m}\left(\frac{1+\gamma}{\rho_{ij}^{\,m}+\gamma} - 2\right) \quad (12)$$

where ϵ_{ij} is the potential well depth, $\rho_{ij} = R_{ij}/R_{ij}^0$ with R_{ij} as the $i-j$ separation and R_{ij}^0 the minimum energy distance. Following Halgren, we used fixed values of $n = 14$, $m = 7$, $\delta = 0.07$,

TABLE 4: Water Dimer Stationary Point Structures and Energies

	ΔE (kcal/mol)		O···H (Å)	
	AMOEBA	ab initio[a]	AMOEBA	ab initio[a]
A	0.00	0.00	1.935	1.949
B	0.57	0.52	1.970	1.972
C	1.22	0.70	2.322	2.280
D	2.02	1.79	2.488	2.515

[a] Reference 93. Structures *a*, *b*, *c*, and *d* in the table correspond to structures 1, 2, 4, and 9 from the reference, respectively.

TABLE 5: Second Virial Coefficient, $B_2(T)$ (L/mol), at Various Temperatures

T (*K*)	expt[a]	AMOEBA	T (*K*)	expt[b]	AMOEBA
298	−1.158	−1.058 ± 0.025	423	−0.275	−0.262 ± 0.009
310	−0.966	−0.877 ± 0.019	448	−0.240	−0.216 ± 0.007
323	−0.816	−0.737 ± 0.015	473	−0.201	−0.181 ± 0.006
336	−0.696	−0.628 ± 0.012	523	−0.150	−0.132 ± 0.004
360	−0.526	−0.474 ± 0.008	573	−0.116	−0.099 ± 0.003
380	−0.428	−0.385 ± 0.006	673	−0.074	−0.061 ± 0.002
400	−0.356	−0.320 ± 0.005	773	−0.050	−0.038 ± 0.003

[a] Reference 95. [b] Reference 96.

and $\gamma = 0.12$. For heterogeneous atom pairs, the combining rules used are

$$R_{ij}^0 = \frac{(R_{ii}^0)^3 + (R_{jj}^0)^3}{(R_{ii}^0)^2 + (R_{jj}^0)^2} \quad \text{and} \quad \epsilon_{ij} = \frac{4\epsilon_{ii}\epsilon_{jj}}{(\epsilon_{ii}^{1/2} + \epsilon_{jj}^{1/2})^2} \qquad (13)$$

The buffered 14−7 function yields a repulsive region softer than the Lennard-Jones 6−12 function but steeper than typical Buckingham exp-6 formulations. The buffered 14−7 form was found to outperform Lennard-Jones and Buckingham potentials in simultaneously reproducing gas phase ab initio results and liquid thermodynamic properties of noble gases and a series of diatomic species.[53,54]

Repulsion−dispersion parameters are placed on both oxygen and hydrogen atoms. Analysis of a series of ice and crystalline hydrate neutron diffraction structures culminated in a set of four linear impenetrability constraints.[55] Together, these constraints suggest a role for anisotropic repulsion, beyond the directionality of hydrogen bonding electrostatics, in water−water interactions. However, since the introduction of "disappearing hydrogen" models,[56] most water potentials have included only a single repulsion−dispersion site. In many cases, the remaining vdW site at the water oxygen atom carries parameters inconsistent with the vdW parameters used by corresponding parametrizations for divalent oxygen atoms in general organic molecules.

The R and ϵ for O and H are chosen to be consistent with AMOEBA force field values for other molecules. The final values have been determined to simultaneously reproduce dimer energy and geometry and liquid density and internal energy, as shown in Table 1. In addition, the hydrogen vdW centers are translated along the O−H bond toward oxygen by 9% of the bond length prior to computation of R_{ij}, a "reduction factor" of 0.91. This displacement only applies to vdW interactions and was optimized to better reproduce different water dimer configurations. The use of reduction factors to move hydrogen sites off of the nuclear position dates from early work on the hydrogen molecule by Stewart et al.[57] Detailed analysis of the X-ray structures of crystalline glycylglycine and sulfamic acid also supports the need to shift hydrogen centers toward the attached heavy atom.[58] A similar scheme has been used successfully by the MM3 force field.[50]

TABLE 6: Water Cluster Equilibrium Properties: Dissociation Energy D_e (kcal/mol), O−O Distance r_{O-O} (Å), O..H−O Angle θ (degree), Average Molecular Dipole $\langle\mu_{mol}\rangle$ (debye), and Total Dipole μ_{tot} (Debye)

		POL5/TZ	TTM2-R	TTM2-F	AMOEBA	ab initio	expt
trimer	D_e	13.42	15.59	15.90	15.32	15.8[a]	
cyclic	$\langle r_{o-o}\rangle$	2.901	2.804	2.800	2.806	2.793[c]	2.845[g]
	$\langle q\rangle$				151.5	150.1[a]	152[d]
	$\langle\mu_{mol}\rangle$	2.22			2.29	2.31[b]	
	μ_{tot}	1.21			1.09	1.14[c]	
tetramer	D_e	25.53	27.03	27.54	27.70	27.6[f]	
cyclic	$\langle r_{o-o}\rangle$	2.769	2.767	2.765	2.760	2.738[c]	2.789[g]
	$\langle\theta\rangle$				168.0	167.7[e]	
	$\langle\mu_{mol}\rangle$	2.47			2.55	2.56[b]	
	μ_{tot}	0.00			0.00	0.00[c]	
pentamer	D_e	34.11	36.05	36.69	36.51	36.3[f]	
cyclic	$\langle r_{o-o}\rangle$	2.742	2.752	2.750	2.756	2.724[c]	2.765[g]
	$\langle\theta\rangle$				176.3	174.0[e]	
	$\langle\mu_{mol}\rangle$	2.57			2.64	2.67[b]	
	μ_{tot}	1.19			0.92	1.04[c]	
hexamer	D_e	41.85	45.11	45.86	45.89	45.9[f]	
prism	$\langle r_{o-o}\rangle$	2.792			2.844	2.840[c]	
	$\langle\mu_{mol}\rangle$	2.52			2.60		
	μ_{tot}	2.91			2.57	2.77[c]	
hexamer	D_e	41.78	45.62	46.46	45.88	45.8[f]	
cage	$\langle r_{o-o}\rangle$	2.783			2.797	2.807[c]	2.820[g]
	$\langle\mu_{mol}\rangle$	2.49			2.58	2.64[b]	
	μ_{tot}	2.44			2.16	2.01[c]	
hexamer	D_e	42.46	45.14		45.77	45.6[f]	
book	$\langle r_{o-o}\rangle$	2.788			2.776	2.766[c]	
	$\langle\mu_{mol}\rangle$	2.55			2.63		
	μ_{tot}	2.45			2.29	2.49[c]	
hexamer	D_e	41.79	44.28	45.03	44.81	44.8[f]	
cyclic	$\langle r_{o-o}\rangle$	2.737	2.746	2.746	2.753	2.714[c]	2.756[g]
	$\langle\theta\rangle$				178.7	177.5[e]	
	$\langle\mu_{mol}\rangle$	2.62			2.70	2.70[b]	
	μ_{tot}	0.02			0.00	0.00[c]	

[a] Reference 142. [b] Reference 146. [c] Reference 98. [d] Reference 149. Distances from Figure 1, scaled by 0.977 to correct for the center-of-mass. [e] Reference 150. [f] Reference 97. [g] Reference 151. Average distances for cyclic forms from eq 20, and the cage hexamer is 0.064 Å greater than cyclic hexamer.

Electrostatics. The permanent multipole moments on each atom were computed via distributed multipole analysis (DMA)[59] at the MP2/aug-cc-pVTZ level and the experimental geometry of the gas-phase monomer. The atomic multipoles were not adjusted from the ab initio values, except for the atomic quadrupole components which were scaled by a factor of 0.73 as discussed below in the section on dimer properties.

The atomic polarizabilities in Table 1 are those developed by Thole[42] for use with the polarization damping scheme described previously. The damping factor in eq 1, a, was originally set to 0.572 by Thole after optimizing the fit to a set of experimental molecular polarizabilities. In agreement with Burnham et al.,[26] we have found that the polarization energy, which was not considered by Thole in the original development of his dipole polarizability model, is much more sensitive to this parameter than is molecular polarizability. In our model, a is reduced to 0.39 based on a fit to water cluster energies. As a result, the average molecular polarizability of water changes from the original 1.414 to 1.408 Å^3 for our value of the damping factor.

Computational Details

Ab initio calculation at the MP2/aug-cc-pVTZ level was performed on a water monomer at the experimental geometry using Gaussian 98.[60] All empirical potential calculations were performed using the TINKER modeling package.[61] Cluster structures were optimized, without any constraints, to a rms

TABLE 7: Liquid Water Properties at Room Temperature

	ρ, g/cm^3	ΔH_V, kcal/mol	e_0	D, 10^5 cm^2/s	$B_2(T)$, L/mol	C_V, cal/(mol·K)
POL5/TZ	0.997	10.51	98 ± 8	1.81	−0.680	22 (C_P)
TTM2-R	1.046	11.80		2.23		
AMOEBA	1.0004 ± 0.0009	10.48 ± 0.08	81 ± 10[a]	2.02 ± 0.05	-1.058 ± 0.032	28.4 ± 2.0[c]
			82 ± 13[b]			(20.9 ± 1.4)
Expt	0.9970[e]	10.51[f]	78.3[g]	2.3[h]	−1.158	17.8

[a] Values from a droplet simulation without cutoffs. [b] Values from a periodic MD simulation using Ewald summation for long-range electrostatics. [c] Values taken from an MD simulation. The value in the parenthesis is from the simulation of a rigid version of the water model, to illustrate the quantum correction to intramolecular flexibility. [d] Reference 152. [e] Reference 95. [f] Reference 108. [g] Reference 103.

TABLE 8: Vibrational Frequencies (cm^{-1}) of Gaseous and Liquid Water

	bending	symmetric stretching	asymmetric stretching
		Gas Phase	
AMOEBA	1577	3663	3756
expt[a]	1594	3656	3755
		Liquid	
AMOEBA	1728	3503	3625
expt[b]	1668	3546	
expt[c]		3466	

[a] Reference 105. [b] Reference 153. The O−H stretch frequency given as the centroid of the stretch band obtained from a neutron scattering study. [c] Reference 154. The frequency reported is an estimate taken from Figure 6 of the peak position of the dominant Gaussian fit to the stretch band.

gradient per atom of 0.0001 kcal/mol/Å with induced dipoles converged to 1×10^{-6} D rms. Second virial coefficients were computed via a procedure similar to that described by Millot et al.[37] At a given dimer center-of-mass separation, the average interactions (Mayer function, mean square force and torque) were sampled over various orientations of the two water molecules. Because the AMOEBA model is flexible, changes in the water geometry were also allowed. A numerical integration of all such interactions over a range of separations, from 0.7 to 16 Å with variable step size, led to the classical second virial coefficient. First-order quantum corrections consisting of both translational (force) and rotational (torque) contributions are included in the results. These corrections are always positive and become more significant at lower temperatures.

Liquid calculations were performed via molecular dynamics simulation of a cubic box approximately 18.643 Å on a side containing 216 water molecules. Ewald summation was used to handle electrostatic interactions, and an atom-based switching window at 12 Å was applied to cutoff the vdW interactions. Integration of the equations of motion was performed via a modified Beeman algorithm using a 1.0 fs time step. The induced dipoles were converged to 0.01 D rms. Unless otherwise specified, a Berendsen weak-coupling thermostat and barostat were used.[62] Molecular dynamics simulation of the reference gas-phase employed stochastic dynamics with a time step of 0.1 fs.

The self-diffusion coefficient of liquid water was evaluated from the constant pressure and temperature dynamics trajectory using the Einstein formula

$$D = \lim_{t\to\infty} \frac{\mathrm{d}}{\mathrm{d}t} \langle |\mathbf{r}(t) - \mathbf{r}(t_o)|^2 \rangle \tag{14}$$

The ensemble average of the mean-square displacement (MSD) is realized by averaging over different time origins t_o. In practice, D was computed from the slope of the MSD collected during a single 1.5 ns *NPT* run. Similarly, the momentum transport coefficient, or viscosity, can be calculated from computer simulations using the Einstein-Helfand relation[63,64]

$$\eta = \frac{V}{2k_B T} \lim_{t\to\infty} \frac{\mathrm{d}}{\mathrm{d}t} \langle (\int_0^t P_{\alpha\beta}(t')\,\mathrm{d}t')^2 \rangle \tag{15}$$

where $P_{\alpha\beta}$ are the off-diagonal components of the pressure tensor as derived in the Appendix. An ideal fluid has no viscosity, corresponding to off-diagonal pressure components of zero. The average of the three off-diagonal components was recorded at every time step, and the resulting ensemble average of the above pressure integral was obtained from a 500 ps constant volume and temperature MD trajectory. The average viscosity was estimated from the slope of a plot of the ensemble average of the pressure integral vs time over the first 3 ps.

The heat capacity of water was estimated from[65]

$$C_V = C_V^K + C_V^\Phi \tag{16}$$

The ideal gas term, C_V^K, is $3Nk/2$, where $3N$ is the total number of degrees of freedom within a flexible all-atom model containing N total atoms. For a rigid water model, $3N$ should be replaced by $6M$, where M is the number of molecules. The nonideal gas term can be evaluated from the potential energy fluctuation in the microcanonical (*NVE*) ensemble[66,67]

$$C_V^\Phi = \frac{k_B \langle \delta\Phi^2 \rangle_{ME}}{(k_B \langle T \rangle)^2 - 2\langle \delta\Phi^2 \rangle_{ME}/3N} \tag{17}$$

Alternatively, it can be computed in the canonical ensemble using the corresponding formula.[65] Berendsen's weak-coupling thermostat generates an ensemble intermediate between canonical and microcanonical; however, for convenience, we use *NVT* and *NPT* to represent constant volume and constant pressure simulations, respectively. Unlike average quantities such as density, energy, etc., fluctuations are ensemble dependent.[65] When the Berendsen weak-coupling thermostat is used during simulation, a modified formula for C_V^Φ has been given by Morishita[68]

$$C_V^\Phi = \frac{k_B \langle \delta\Phi^2 \rangle_{WE}}{(k_B T)^2 - 2\sqrt{\langle \delta K^2 \rangle_{WE} \langle \delta\Phi^2 \rangle_{WE}}/3N} \tag{18}$$

The static dielectric constant was assessed via two different approaches. First, it was computed from the fluctuation of the total dipole moment of the simulation cell as sampled during MD simulation using Ewald summation with the tin-foil boundary condition[69,70]

$$\epsilon_0 = 1 + \frac{4\pi}{3k_B TV} (\langle M^2 \rangle - \langle \mathbf{M} \rangle \cdot \langle \mathbf{M} \rangle) \tag{19}$$

where $\mathbf{M} = \Sigma_i(\boldsymbol{\mu}_i + q_i\mathbf{r}_i)$ is the cell dipole moment, V is the volume of the simulation cell, and T is the temperature. In practice, the ensemble average is estimated by a simple cumulative time average. The $\langle\mathbf{M}\rangle\cdot\langle\mathbf{M}\rangle$ term in the above equation is often neglected because the ensemble average of the total cell dipole for a disordered liquid approaches zero for long simulation time (>1 ns).

In a separate calculation, the static dielectric constant of AMOEBA water was determined from simulation of a droplet in a vacuum.[71−73] A microscopic droplet was created using a soft spherical potential.[74] The droplet contains an inner sphere that behaves like bulk water, and an outer shell in contact with vacuum. The dielectric constants, ϵ_1 for the inner sphere and ϵ_2 for the outer region, are related to the fluctuation of the total dipole moment of the inner sphere by

$$\frac{\langle M^2\rangle}{k_B T r_1^3} = \frac{(\epsilon_1 - 1)[(1 + 2\epsilon_2)(2 + \epsilon_2) - 2(r_1/r_2)^3(1 - \epsilon_2)^2]}{(\epsilon_1 + 2\epsilon_2)(2 + \epsilon_2) - 2(r_1/r_2)^3(1 - \epsilon_2)(\epsilon_1 - \epsilon_2)} \tag{20}$$

where r_1 and r_2 are the radius of inner sphere and outer shell, respectively. The above equation can be solved for the dielectric constant by invoking the approximation $\epsilon_1 \approx \epsilon_2$.[73]

The experimental structure of ice Ih was constructed by Hayward and Reimers[75] with two hydrogen atoms near each oxygen atom, one hydrogen along the line joining each pair of neighboring oxygens, and the disordered protons arranged such that the unit cell has near zero dipole and quadrupole moments. A $4 \times 3 \times 2$ supercell ($a = 18.02824$ Å, $b = 23.41938$ Å, and $c = 14.72000$ Å) was chosen as the unit cell with the hexagonal periodicity converted to the equivalent pseudo-orthorhombic form for convenience. The unit cell for proton-ordered ice XI was a $4 \times 3 \times 3$ supercell with $a = 18.0080$ Å, $b = 23.3940$ Å, and $c = 21.9840$ Å. It was constructed with the TINKER Crystal program using the experimental fractional coordinates[76] as input.

The standard error for various properties is calculated from the following equation:

$$\mathrm{STDERR} = \frac{\sigma}{\sqrt{\tau_{\mathrm{run}}/\tau_{\mathrm{b}}}} \tag{21}$$

where σ is the standard deviation of the computed property obtained from the simulation, and τ_{run} and τ_{b} are the simulation length and correlation time estimated from the statistical inefficiency, respectively (see Allen and Tildesley,[65] page 193).

Results and Discussion

Gas Phase. A comparison of the experimental, ab initio and AMOEBA calculated molecular dipole moment, quadrupole moment, and polarizability of a single isolated water molecule is given in Table 2. Two other recently developed water models, POL5/QZ[14] and TTM2-R,[28] are also listed. POL5/QZ is a fluctuating charge 5-site model with induced dipole, whereas TTM2-R is a 4-site fixed charge model with induced dipole. Two sets of AMOEBA values are listed, corresponding to the ideal bond angle of 108.5° and the experimental angle of 104.52°.[77] AMOEBA atomic multipole parameters were obtained at the experimental angle. However, classical models with intramolecular flexibility, polarizable or not, tend to exhibit a reduced H−O−H bond angle upon moving from the gas phase to condensed phases,[78−82] a trend opposite to the experimental observation. Flexible models have been criticized for their inability to correctly describe the dependence of molecular multipole moments on water vibrations.[83−86] Recently, Burnham and Xantheas[28] have suggested that the incorrect dipole moment derivative with respect to O−H stretching is responsible for the reduction of the H−O−H bond angle in the condensed phase. Traditional flexible models have the molecular dipole moment derivative ($\partial\mu/\partial$r) along the O−H bond. In contrast, experiments indicate that the direction of the ($\partial\mu/\partial$r) vector should lie >20° outside the O−H bond in the gas phase but near to the O−H bond direction in ice.[87] In the AMOEBA model, the polarization is dependent upon the water geometry only in the presence of an external field; that is, the intramolecular polarization induced by geometry variation is missing in the absence of an external field. Although it may be possible to correct this deficiency via coupling of electrostatic parameters to intramolecular geometry,[28,88−90] we have chosen a solution adopted by other flexible potentials[82,91] of increasing the ideal bond angle so that water molecules will assume the correct average geometry in the liquid. As can be seen in Table 2, the increase in the ideal angle value from 104.52° to 108.5° results in relatively small changes in the monomer properties.

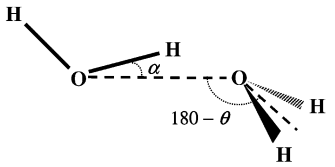

Figure 2. Water dimer equilibrium structure. The angle a measures the deviation of the donor hydrogen from the O···O direction. The "flap angle", θ, is the angle between the extended O···O vector and the bisector of the H−O−H angle of the acceptor molecule.

The equilibrium structure of the AMOEBA water dimer is compared with experimental and ab initio results in Table 3. The water dimer, in particular, represents a case where ab initio results are preferred over experimental values in calibrating a new empirical potential. Correction of the experimentally determined ΔH of association in hot vapor and the microwave structure for anharmonic vibration and temperature effects is problematic.[92] In recent years, various high-level ab initio calculations carried out by different groups have converged with regard to the water dimer binding energy and equilibrium structure. The AMOEBA dimer results are in excellent agreement with these consensus theoretical values. During the parametrization process, we noticed that the flap angle, θ in Figure 2, is correlated with the monomer quadrupole component directed along the H−O−H bisector, Q_{zz}. For example, multipole moments taken directly from the DMA of the monomer result in a flap angle of about 70°. In the AMOEBA water parameters, the oxygen and hydrogen atomic quadrupoles defined in their local frames are scaled to 73% of the DMA values. This scaling leads to a larger Q_{zz} component of the molecular quadrupole which in turn reduces the flap angle to 57°, in agreement with both ab inito and experimental results. It is interesting that the TTM and TTM2-R potentials, which give a very similar flap angle, also exhibit a large Q_{zz} component.

In addition to the equilibrium structure, other stationary points on the water dimer potential surface have been examined. The relative binding energies and hydrogen bonding distance for the equilibrium structure and the three transition state structures are given in Table 4. AMOEBA binding energies exhibit the same trend as computed by ab initio theory[93] for the different structures. The value of the hydrogen vdW reduction factor is critical in fitting all of the dimer orientations simultaneously, as it effectively provides an extra degree of freedom for

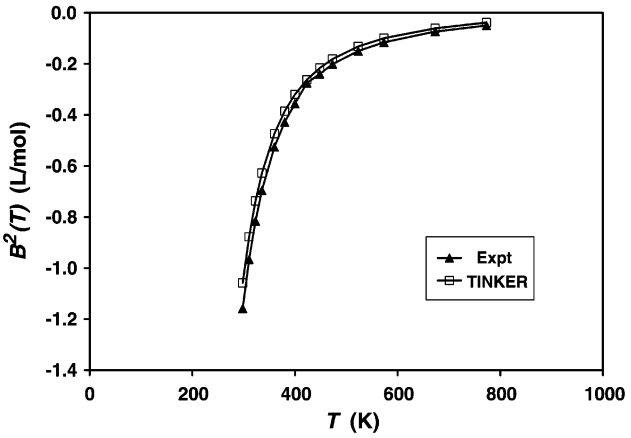

Figure 3. Second viral coefficient of water at various temperatures. The quantum-corrected AMOEBA values are in good agreement with experimental data, even as the curve becomes steep in the low-temperature region.

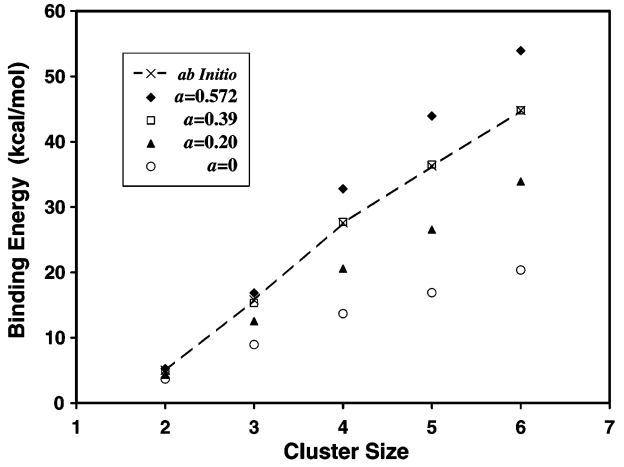

Figure 4. Water cluster binding energies computed with different polarization damping factors. A linear piecewise curve is drawn through the ab initio results, which are taken from refs 97 and 142. Hexamer energies shown are for the cyclic configuration. The value of $a = 0.572$ was originally suggested by Thole, whereas the AMOEBA water model uses $a = 0.39$. The $a = 0.2$ curve shows the effect of overdamped polarization. The $a = 0$ data corresponds to an AMOEBA model without any contribution from polarization effects.

adjustment of vdW anisotropy. It is impossible to determine a unique hydrogen reduction factor based solely on the equilibrium structure with its head-on hydrogen bond,

It has been reported that the polarizable ASP-W4[37] and TTM2-R[27] water models are successful in predicting the second virial coefficients above 400 K. It seems essential for a polarizable potential to be able to reproduce the second virial coefficients, which provide a measure of the accuracy of the full dimer potential surface. In this study, the second virial coefficients were computed as described previously.[37] A series of calculations were carried out at several temperatures between 298 and 800 K. At each temperature, five independent calculations were used to obtain the average second virial coefficient and its standard error. As shown in Figure 3 and Table 5, the second virial coefficients computed by the AMOEBA model are in excellent agreement with experiment over the whole temperature range. The deviation from the experimental value increases as temperature decreases, with a maximum absolute error of 0.1 L/mol at 298 K. At all temperatures, AMOEBA values are systematically less negative than the experimental measurements. At 298 K, the total first-order quantum correction, 90% of which is due to the rotational component, amounts to 35% of the magnitude of the virial coefficient. It has been suggested that at lower temperatures the second order corrections, which happen to be negative, may become significant.[94] Another possible source of discrepancy is uncertainty in the experimental measurements, which also increases at lower temperatures. For example, at 423 K, the available experimental values for $B_2(T)$ range from -0.294[95] to at least -0.275 L/mol.[96]

Clusters from the trimer through the hexamer have been analyzed using the AMOEBA water model. Following the calculations of Stern et al.,[14] we have investigated the cyclic trimer, tetramer, and pentamer, as well as prism, cage, book, and cyclic configurations of the hexamer. MP2/CBS energies and structures for these clusters became available recently.[97] All clusters were subjected to full geometry optimization without any constraints. The binding energies, individual and average O−O distances, O···H−O angle, average molecular dipole moments, and total dipole moments of the clusters from various models are collected in Table 6. The AMOEBA binding energies are in excellent agreement with the ab initio results. The rms error in the total binding energy for our model is only 0.21 kcal/mol with a maximum error of 0.48 kcal/mol for the trimer. The estimated accuracy of MP2/CBS binding energies is 0.2 kcal/mol.[97] For the hexamer clusters, the ordering of the MP2/CBS binding energies is prism > cage > book > cyclic, exactly as computed with the AMOEBA model. However, both the TTM2-F and TTM2-R models find the cage configuration to be more stable than the prism form by about 0.5 kcal/mol.

The predicted cluster geometries are in generally good agreement with ab initio results. For the same set of cyclic clusters, both the AMOEBA model and MP2/TZ2P++ optimization[98] yield average O···O nearest neighbor distances that decrease with increasing cluster size. However, our O···O distances are systematically longer than ab initio estimates. A similar overestimation of O···O distance is also observed for the TTM2-F and TTM2-R models.[28]

The water clusters provide a critical calibration for the increasing importance of polarization as one moves from the gas-phase toward bulk phases. As discussed earlier, the value of the Thole damping factor, a, controls the strength of short-range polarization interactions. Smaller values of a correspond to stronger damping of polarization. Figure 4 shows the binding energy as a function of cluster size for different values of a. The value $a = 0.572$ originally suggested by Thole leads to an overestimation of binding energies that becomes more substantial for the larger clusters. This is due to insufficient damping resulting in overly large polarization energies. Conversely, a value of $a = 0.2$ overdamps the polarization resulting in systematic underestimation of cluster energies. With our chosen value of $a = 0.39$, the AMOEBA water model quantitatively reproduces the nonadditivity of the binding energy data. Our current experience indicates the same value is optimal for bulk phases of water, as well as for a variety of other small molecules.

Liquid Phase. Thermodynamic properties of liquid water at room temperature have been sampled via MD simulations using the AMOEBA model. Both constant pressure ($P = 1$ bar) and constant volume ($\rho = 0.997$ g/cm^3) simulations have been carried out at 298 K, with results summarized in Table 7. The temperature dependence of liquid water properties has also been studied, and will be reported in a later publication.

The average liquid density at room temperature obtained from a 1.5 ns *NPT* simulation is 1.0004 g/cm^3, 0.3% higher than the experimental density of 0.9970 g/cm^3. Similarly, a 2 ns *NVT* simulation at the experimental density yields an average pressure of -66 ± 14 bar. The heat of vaporization is computed from

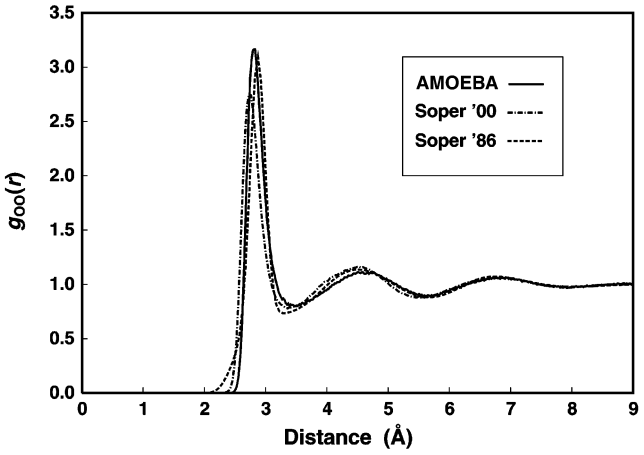

Figure 5. O···O radial distribution function for AMBOEBA liquid water at 298 K, compared with two neutron scattering derived experimental curves from Soper's group. The '00 curve is a revised analysis of '86 experimental data as discussed in the text.

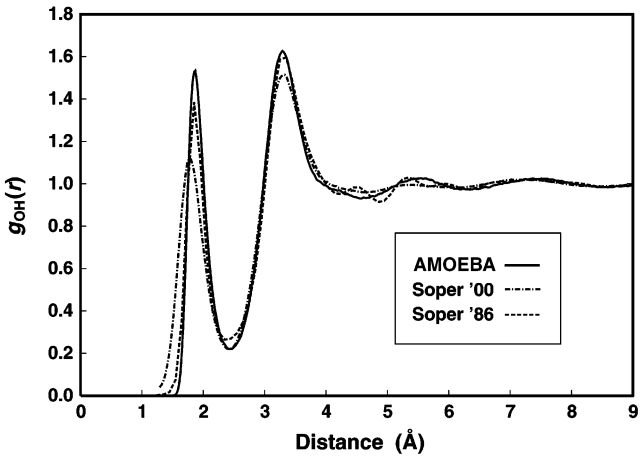

Figure 6. O···H radial distribution function for AMOEBA liquid water at 298 K, compared with two neutron scattering derived experimental curves from Soper's group.

the potential energy difference between liquid and gas phases, assuming water vapor to be an ideal gas

$$\Delta H_V = -\Delta E + \Delta PV = -E_{liq} + E_{gas} + RT \qquad (22)$$

The potential energy of the gas as obtained from stochastic dynamics simulation of a monomer at room temperature using a small time step of 0.1 fs is $E_{gas} = 0.89$ kcal/mol. The potential energy of the liquid from the *NPT* simulation is −9.00 kcal/mol. Thus, the heat of vaporization at 298 K is 10.48 kcal/mol, close to the experimental value of 10.51 kcal/mol.[95]

To characterize the liquid structure, radial distribution functions (RDFs) have been sampled from the *NPT* dynamics simulation for O···O, O···H, and H···H pairs. Until recently, RDFs inferred from experimental measurements had displayed significant disagreement. Sorenson et al.[99] provide a summary of experimental and simulated $g_{OO}(r)$ results obtained over many years. Two groups have now reported almost identical $g_{OO}(r)$ curves based on independent analyses of neutron scattering[100] (Soper 2000) and X-ray experiments,[99] which represent the best $g_{OO}(r)$ estimates currently available. Computed RDFs for AMOEBA water, plotted in Figures 5−7, have been compared with Soper's 2000 curves as well his earlier 1986 results.[101] The Soper 2000 results are derived from empirical potential

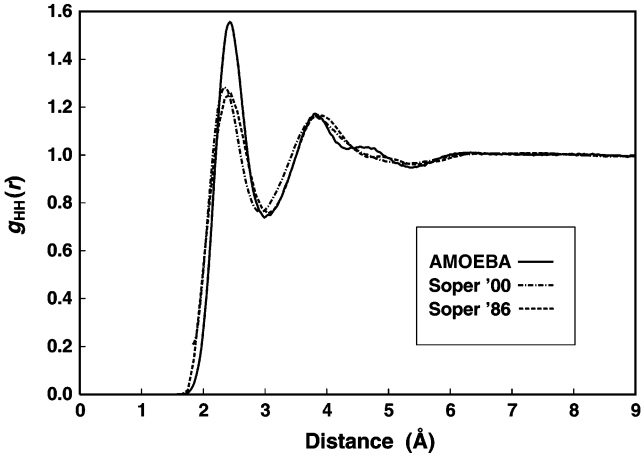

Figure 7. H···H radial distribution function for AMOEBA liquid water at 298 K, compared with two neutron scattering derived experimental curves from Soper's group.

structure refinement (EPSR) using two sets of experimental data: pulsed neutron time-of-flight diffraction data and an older reactor neutron diffraction data set. The latter is the same data from which the 1986 results were derived via a maximum entropy data analysis. The $g_{OO}(r)$ of Sorenson et al. from X-ray data is not shown in Figure 5 as it is nearly indistinguishable from the Soper 2000 result. The position of the first peak of the AMOEBA $g_{OO}(r)$ is 2.81 Å, 0.08 Å greater than that of the Soper 2000 RDF, but 0.07 Å smaller than the position of the corresponding peak in the Soper 1986 RDF. A recent quantum mechanical MD study estimated the first peak of $g_{OO}(r)$ in the liquid to be at 2.78 Å at 318 K.[102] However, the quantum MD values are uncertain due to the short simulation length of 10 ps and small system size of 64 molecules. The first peak of the AMOEBA RDF has a height about 0.4 higher than the Soper 2000 data. The experimental uncertainty in this peak height is large, with a standard deviation of 0.32 as reported by Soper.[100] Sorensen et al. have suggested that the experimental quantities reliable enough to serve as benchmarks for comparison with simulation are the position of the first peak and the peak and trough heights of the second and third peaks. They also state that the height of the first peak has a lower bound of 2.6 according to their X-ray analysis.[99] The depths of the first and second trough as well as the second peak height of the AMOEBA $g_{OO}(r)$ agree very well with the Soper 2000 RDF, except our curve is systematically shifted slightly to the right. All attempts to move the RDF distribution to the left via parameter changes cause the bulk internal energy to become too low and the O···O distance of the water dimer to become too short. This trend is also observed for the polarizable POL5/TZ and POL5/QZ potentials.[14] Another rigid polarizable model, TTM2-R,[27] is reported to be successful in reproducing the experimental $g_{OO}(r)$. However, the TTM2-R model yields a density of 1.046 g/cm^3 and heat of vaporization of 11.8 kcal/mol at 298 K, values that are 5% and 12% greater than experimental measurements, respectively. The anomalously high density and low energy of this model serve to shift the $g_{OO}(r)$ curve to the left and sharpen its structure.The first peaks of the $g_{OH}(r)$ and especially the $g_{HH}(r)$ of AMOEBA water are also too high in comparison with the Soper 2000 data. The positions of the first peaks for both curves are again slightly to the right of the corresponding Soper 2000 peak positions but agree very well with the Soper 1986 data. Features beyond the first peaks also are in excellent agreement with the 1986 experimental curves.

The self-diffusion coefficient computed from *NPT* MD simulation is 2.02×10^{-5} cm^2/s, which is slightly lower than the experimentally measured value of 2.3×10^{-5} cm^2/s.[103] The viscosity of AMOEBA water is 1.35 cp. This value is much higher than the experimental measurement of 0.89 cp at 298 K[95] but is consistent with the low self-diffusion coefficient of the current model. To achieve the experimental viscosity, a diffusion coefficient of at least 2.6×10^{-5} cm^2/s is required, as indicated by a series of simulations of SPC and SPC/E water by Smith and van Gunsteren.[104]

Using Berendsen coupling and the Morishita formula (eq 18), the constant volume dynamics simulation led to a heat capacity of 28.4 kcal/mol/K using the AMOEBA flexible water model. This result is in good agreement with a value of 27.6 kcal/mol/K obtained from a 200 ps *NVE* dynamics trajectory using eq 17. To ensure correct fluctuations during *NVE* simulation, it is necessary to enforce tight convergence on the mutual induced dipole calculations (e.g., 10^{-6} D rms).

It is well-known that classical approximation of the intra- and intermolecular vibrations overestimates the heat capacity compared with a quantum oscillator model.[105] Levitt et al.[82] proposed a correction of 6 kcal/mol/K should be subtracted from the heat capacity obtained from energy fluctuations of a classical flexible model, whereas for a rigid water model, the correction is negligible. To validate Levitt et al.'s proposed correction, we repeated the Berendsen thermostat simulation with the water geometry constrained via the Rattle algorithm.[106] The resulting heat capacity was reduced to 20.9 kcal/mol/K, a value much closer to the experimental C_v of 18 kcal/mol/K. The heat capacity can also be estimated via differentiation of internal energy with respect to temperature, which should yield a value independent of fluctuations.[107] As will be discused in a later publication, C_P obtained in this manner for the flexible AMEOBA model is ~21 kcal/mol/K.

The previously mentioned 2 ns *NVT* trajectory was utilized to calculate the dielectric constant from Ewald simulations, resulting in a value of 82 at 298 K. Meanwhile, a 2 ns *NVT* simulation was carried out on a 12 Å radius droplet containing 242 molecules. The dielectric constant calculated from the droplet simulation depends on the choice of inner sphere radius r_1. An outer shell of thickness 4−6 Å is necessary to achieve a converged ϵ, in agreement with previous observation.[74] A value of 6 Å for r_1 in this work leads to a final dielectric constant of 81.

Thus, the dielectric constants determined by Ewald summation and from a vacuum droplet are both in very good agreement with the experiment value of 78.3.[108] It has been suggested that the water dielectric constant correlates with the average molecular dipole moment in the liquid and that an average moment exceeding 2.6 D would lead to a significantly overestimated ϵ_o.[109] However, the average molecular dipole moment in liquid water is not known exactly from either experiment or theory. An early theoretical estimate based on an induction model resulted in an a value of 2.6 D for ice Ih,[110] which unfortunately has been mistakenly used as the "experimental" value for *liquid* water over the years. A recent ab initio MD simulation study suggested an average liquid-phase value as high as 2.95 D.[111] Meanwhile, Batista et al.[112] reported a variation from 2.3 to 3.1 D for the average molecular dipole in ice Ih depending on the scheme used to partition the ab initio electron charge density. On the other hand, Höchtl et al.[113] argued the H−O−H bond angle instead of the molecular dipole moment is the principle determinant of ϵ_o, which they supported with simulation results from of a number of SPC/TIP3P hybrid models. They found that two models with almost identical molecular dipole moments, but different geometries, gave static dielectric constants that differed by a factor of 2.

TABLE 9. Ice Properties. Density and Lattice Energy of Ice 1h and Ice XI

	ρ (g/cm^3)			lattice energy		
	TTM2-R	AMOEBA	expt	TTM2-R	AMOEBA[b]	expt[a]
ice 1h ($P6_3/mmc$)	0.942	0.916	0.931[c]	14.69	14.31	14.1
ice XI ($Cmc2_1$)		0.923	0.934[d]		14.18	14.1

[a] Experimental value for lattice at 0 K after removal of zero-point energy. [b] Values from full crystal minimization starting from the experimental structure. [c] Reference 155. Value determined at a temperature of 100 K. [d] Reference 156. Value determined at a temperature of 5 K.

The AMOEBA model gives an average dipole moment of 2.78 D in the liquid, over 50% greater than the gas phase moment of 1.85 D. The larger value in the liquid is a direct result of dipole polarization. The distribution of molecular moments is nearly Gaussian with a width at half-height of approximately 0.8 D. Meanwhile, the H−O−H angle is reduced from the ideal AMOEBA value of 108.5° in the gas phase to an average of 105.4 ± 4.4° in the liquid. The accepted experimental value for the H−O−H angle in liquid water is 106.1 ± 1.8°,[114] whereas the value suggested by ab initio dynamics simulation is 105.5°.[102] Furthermore, AMOEBA water exhibits an elongation of the O−H bond from 0.9572 Å in the gas phase to 0.9701 ± 0.0245 Å in the liquid. These bond lengths are in excellent agreement with the experimental values of 0.957 Å in the gas[51] and 0.970 Å in liquid water.[114] During the parametrization process, we found that AMOEBA models with 2−3° smaller H−O−H angles and average dipole moments over 2.7 D had dielectric constants greater than 100. This observation tends to confirm the conclusion of Höchtl et al.[113] that the static dielectric constant has a strong dependence on the water geometry, especially the H−O−H angle. The average molecular dipole moment of liquid water, which is obviously affected by changes in water geometry, is probably a secondary factor.

It is well-known that the vibrational frequencies of water shift upon moving from the gas phase to the liquid. The AMOEBA model is not suitable for predicting IR intensities because of inaccuracy in the direction of the dipole moment derivative with respect to O−H bond stretching. However, it is still of interest to see whether the AMOEBA model is able to qualitatively predict the frequency shifts upon phase change. The power spectrum of AMOEBA liquid water was computed from a velocity autocorrelation function acquired from a 2 ps *NVE* dynamics simulation using velocities recorded at every 0.1 fs time step. The results are given in Table 8 together with the corresponding gas phase vibrational frequencies. Upon moving from gas to liquid, AMOEBA water displays the observed blue shift of the bending frequency and red shift of the stretching frequencies. It was pointed out long ago that anharmonic valence terms, such as those included in the AMOEBA model, are needed to sufficiently soften the bond stretches in the liquid phase.[115]

Ice. The ice Ih and XI crystal forms have been modeled using the AMOEBA water potential. Experimental structures were first optimized with fixed cell parameters to a convergence of 0.01 kcal/mol/Å. In Table 9, the lattice energies of the two ice forms, computed as the energy required to infinitely separate the water molecules from the minimized ice geometry, are compared to the reported experimental value of 14.1 kcal/mol at 0 K and

TABLE 10: Energy Decomposition for Water Cluster and Bulk Systems[a]

	valence terms	van der Waals	permanent electrostatics	polarization eletrostatics	total energy	$E_{pol}/(E_{perm}+E_{pol})$	$\langle\mu_{mol}\rangle^b$
dimer	0.019	1.172	−3.033	−0.639	−2.480	0.174	2.02
cyclic trimer	0.082	2.931	−5.995	−2.126	−5.108	0.262	2.29
cyclic tetramer	0.158	4.447	−8.027	−3.503	−6.925	0.304	2.55
cyclic pentamer	0.198	4.735	−8.314	−3.921	−7.302	0.320	2.64
cyclic hexamer	0.223	4.823	−8.441	−4.074	−7.469	0.326	2.70
liquid[c]	1.214	4.494	−10.342	−4.394	−9.028	0.298	2.78
ice Ih[d]	0.670	8.617	−15.260	−7.004	−12.977	0.315	3.09

[a] Energy values are given in kcal/mol per molecule. [b] Average molecular dipole moment in Debye. [c] Values taken from an MD trajectory at 298 K. [d] Values taken from an MD trajectory at 100 K.

zero pressure.[116] The "experimental" value contains a significant amount of zero-point energy correction estimated from intramolecular and lattice vibrations. An energy minimization was also carried out on the structure of ice Ih with all atomic positions and cell parameters subject to optimization. The resulting structure and energy are essentially identical to that from the fixed lattice optimization, whereas cell lengths increased by 0.003 Å on average.

Molecular dynamics simulations of the two ice forms were performed at experimental temperature and pressure. The structures were equilibrated via 300 ps *NPT* simulations at 1 atm and 5 K for ice XI and 100 K for ice Ih. During the MD simulations, the cell sizes were allowed to deform isotropically according to Berendsen's barostat. The equilibrium densities were computed from the dynamics trajectories and are listed in Table 9. In both cases, the AMOEBA ice structures expanded slightly, leading to densities somewhat lower than experiment. The $g_{OO}(r)$ of AMOEBA ice has a first peak at 2.755 Å, in excellent agreement with the experimental average O···O distance of 2.76 Å.[117] The average O−H bond length is 0.9721 ± 0.0144 Å, slightly longer than the liquid but not stretched enough in comparison with 0.985 Å from the neutron diffraction structure of ice.[118] The average H−O−H angle in ice sampled during the MD simulation is 105.1 ± 2.4°, nearly identical to the liquid. Early interpretation of neutron diffraction experiments suggested a D−O−D angle of 109.5° for ice Ih, based on an anomalously long O−D bond length of 1.01 Å.[119] The current best estimate for the H−O−H angle from various experimental observations is 106.6°.[81,117] The average molecular dipole moment of AMOEBA ice is 3.08 D, whereas a recent theoretical estimate from an induction model for ice Ih is 3.09 D.[120]

Conclusion

As the first step in the derivation of a next-generation polarizable force field for biomolecular simulation, a polarizable atomic multipole water model has been developed and validated. The main features of the AMOEBA model include (1) the use of higher-order moments to improve the description of electrostatics and eliminate the need for adding off-atom sites as in the TIP4P and TIP5P models, (2) a modified Thole damping scheme which prevents the short-range polarization catastrophe while providing correct anisotropic molecular polarizabilities, and (3) the presence of nonzero van der Waals parameters and reduction factors on hydrogen atoms which produce an improved molecular "shape". It has been successfully applied to the study of a wide range of properties of gas-phase clusters, liquid water, and ice crystals. The results are generally satisfactory in comparison with results from high-level ab initio theory and experiments. The majority of the many-body effect is adequately accounted for by classical dipole polarization. More importantly, the AMOEBA potential represents a general model built on atomic multipoles and isotropic polarizabilities. The required atomic multipoles are readily obtained from high-level ab initio calculations for model compounds ranging from small organic molecules to dipeptides. The induction model requires only a single isotropic polarizability for each element. Thus, the overall model can be readily extended to development of a transferable force field for a wide range of molecular systems in addition to water.

Considering only the average thermodynamic properties of homogeneous liquid water, the inclusion of explicit polarization in the AMOEBA model seems to provide no immediate advantage over a good fixed charge model such as TIP5P.[6] However, many-body effects in water depend strongly on the environment as indicated by energy decompositions for our model, shown in Table 10. The fraction of the total electrostatic energy due to polarization effects grows gradually with cluster size. In liquid water, which can be viewed as a mixture of cluster geometries, polarization accounts for 29.8% of the total electrostatic energy, about the same as for the cyclic tetramer. Upon moving from the liquid to ice Ih, this fraction increases to 31.5%. The average molecular dipole moment steadily increases from the dimer to larger clusters, to the liquid, and finally to ice Ih. This is another manifestation of the strong variation of many-body effects with environment. It is possible for a nonpolarizable potential to model the average properties of any single system. However, many-body effects such as polarization have to be modeled explicitly and correctly in order to capture the details of water structure and thermodynamics in different environments.

Because of the classical nature of molecular mechanics, quantum effects such as vibrational zero-point energy need to be taken into account in comparing results from classical models with experimental data. As mentioned above, the experimental sublimation energy of ice at 0 K contains zero-point energy that needs to be removed prior to comparison with the classical models. Whalley[116] estimated the correction to the ice lattice energy to be 2.78 kcal/mol by accounting for the shifts in experimental vibrational frequencies upon moving from gas to ice and assigning $1/2h\Delta\upsilon$ to each mode. For liquid water at room temperature, one might expect the magnitude of the quantum correction to be smaller than the ice estimate simply because of the higher temperature. However, the several literature estimates of the quantum correction to the liquid energy are spread over a wide range. In an approach analogous to Whalley's, Owicki and Scheraga[121] estimated the quantum correction due to the classical treatment of inter- and intramolecular vibrations as 0.2 kcal/mol at 298 K. A similar recent analysis by Buch et al. suggests the various components of the correction cancel, resulting in a total correction of only 0−0.1 kcal/mol.[122] From an integration of the quantum harmonic oscillator energy over the simulated liquid spectral density, Lie and Clementi[85] arrived at a correction of 0.93 kcal/mol for the flexible MCYL water model. In a similar fashion, Stern and

Berne[123] obtained a quantum correction as large as 1.7 kcal/mol for the MCDHO model.[36] Path integral[124] quantum simulations where the classical particles were represented by quantized "beads" have been used to investigate quantum effects.[91,123,125,126] These studies show that quantizing a classical model results in faster diffusion,[126] a smaller heat capacity,[91] a broader dipole moment distribution,[123] and less structure in the liquid RDF.[91] The estimated magnitude of the quantum correction varies from 0.8[127] to 1.5 kcal/mol[123] and seems to depend of the underlying classical model and details of the path integral methodology. Mahoney and Jorgensen[91] derived a quantized TIP5P(PIMC) model for use in path integral simulations via reparametrization of the atomic charges in the classical TIP5P model. With the exception of heat capacity, TIP5P(PIMC) was very similar to classical TIP5P in terms of its ability to reproduce a variety of experimental properties. This result indicates that a classical model of liquid water can be parametrized to include most quantum effects implicitly in an average fashion and then directly compared with experimental properties. Our results also indicate the quantum correction in liquid water may be small and can be partially included in parametrization of a classical potential, so we have chosen to neglect any correction of our model.

Burnham and Xantheas[28] proposed a water model with variable charges that account for charge distortion upon change in the intramolecular geometry in the absence of an external field. Their water cluster results display the correct trend in H−O−H angle variation with cluster size. However, the geometry dependent charges were based on a numerical implementation of an 84-term model for the dipole moment surface (DMS) of the water monomer derived from ab initio calculations.[128] There is also evidence that a simple geometry-coupled charge flux scheme can capture the correct dipole derivative and thus the trend of water geometry changes.[129] On the other hand, physical approximations such as dipole induction used by the AMOEBA model and fluctuating charge models[13,130−133] have been mostly applied to describe the response of a molecule or a segment of a large molecule to an external electric field. It is unclear whether such models can be extended easily to account for valence polarization at typical bond distances.

Computational cost is an important consideration for a general potential model. In our hands, the AMOEBA water model is approximately 8 times slower than the TIP3P model for dynamics simulation of a periodic system of 216 water molecules. This comparison was made using the TINKER MD engine with comparable simulation conditions, except that traditional Ewald was used for the AMOEBA model and smooth particle-mesh Ewald[134] (PME) for TIP3P. Even though a relatively loose convergence criterion of 0.01 D rms is enforced at each dynamics step, almost half of the total computational cost is due to the iterative calculation of the induced dipoles. For dynamics calculations, it is possible to greatly reduce this cost by replacing the self-consistent iteration with an extended Lagrangian scheme[13,20,135−138] for estimating the induced dipoles. Because the higher-order moment interactions converge at shorter distances than point charge interactions, multiple-cutoff schemes for the Ewald summation could be utilized to further improve efficiency. There is also the possibility of implementing PME or fast cell multipole methods to handle polarizable multipole interactions in large simulation systems.[139,140]

Acknowledgment. The authors thank Dr. Yong Kong for preliminary work in developing an earlier version of the water model, Dr. Peter Bagossi for the parametrization of related small molecules, and Dr. Alan Grossfield for numerous helpful suggestions and discussions. The TINKER modeling software containing the water model for the AMOEBA force field is available from http://dasher.wustl.edu/tinker/. This work was funded by Grant No. 9808317 from the Computational Biology Activity of the National Science Foundation.

Appendix: Ewald Summation for Polarizable Multipoles

A cell matrix definition[47] suitable for periodic cells of any shape is used to describe the system. Given the vectors forming the three edges of the unit cell, $\mathbf{a}_\alpha = [a_{\alpha 1}, a_{\alpha 2}, a_{\alpha 3}]^T$ for $\alpha = 1, 2, 3$, we define the cell matrix

$$\boldsymbol{A} = [\mathbf{a}_1, \mathbf{a}_2, \mathbf{a}_3] = \{a_{\alpha\beta}\} \text{ for } \alpha, \beta = 1, 2, 3 \tag{23}$$

The atomic coordinates can be expressed in terms of real space vectors

$$\mathbf{r} = \boldsymbol{A}\mathbf{s}, \quad \text{or} \quad r_{j\alpha} = \sum_{m=1}^{3} a_{m\alpha} s_{jm} \quad \text{for} \quad \alpha = 1,2,3 \tag{24}$$

where s_{jm} for $m = 1, 2, 3$ are the fractional coordinates of site j.

The conjugate reciprocal cell matrix is defined as $\boldsymbol{A}^* = [\mathbf{a}_1^*, \mathbf{a}_2^*, \mathbf{a}_3^*]^T$ where each row is a reciprocal cell vector, $\mathbf{a}_\beta^* = [a_{\beta 1}^*, a_{\beta 2}^*, a_{\beta 3}^*]$. The two matrixes satisfy $\boldsymbol{A}^*\boldsymbol{A} = \boldsymbol{I}$, i.e., $a_{\alpha m}^* a_{\beta m} = \delta_{\alpha\beta}$. The reciprocal space vector can be written as $\mathbf{h} = (\boldsymbol{A}^*)^T\mathbf{n}$ where $\mathbf{n} = [n_1, n_2, n_3]^T$ is a vector of integer components.

Let us define the reciprocal lattice vector, $\mathbf{k} = 2\pi\mathbf{h}$. Then, the Ewald summation formulation of the polarization energy is expressed as

$$U^{\text{pol}} = \frac{1}{2}\sum_i \sum_{j>i} \sum_{m=1}^{3} G_{ji}^{\ m}(\mathbf{r}_{ji})\, B_m(\mathbf{r}_{ji}) + \frac{\pi}{V}\sum_{k\neq 0}^{\infty} A_k \sum_i \sum_{j\neq i} f_{ji}^{\text{ind}} \exp(-i\mathbf{k}\cdot\mathbf{r}_{ji}) - \frac{2\xi^3}{3\sqrt{\pi}}\sum_i (\boldsymbol{\mu}_i^{\text{ind}}\cdot\boldsymbol{\mu}_i) \tag{25}$$

where

$$\mathbf{r}_{ji} = \mathbf{r}_j - \mathbf{r}_i$$

$$A_k = \frac{1}{k^2}\exp\left(-\frac{k^2}{4\xi^2}\right)$$

$$f_{ji}^{\text{ind}} = i\boldsymbol{\mu}_i^{\text{ind}}\cdot\mathbf{k}(q_j - i\boldsymbol{\mu}_j\cdot\mathbf{k} - \boldsymbol{Q}_j:\boldsymbol{K}) - i\boldsymbol{\mu}_j^{\text{ind}}\cdot\mathbf{k}(q_i + i\boldsymbol{\mu}_i\cdot\mathbf{k} - \boldsymbol{Q}_i:\boldsymbol{K})$$

The three terms in the above equation for U^{pol} are the real space, reciprocal space, and self-interaction components of the Ewald sum, respectively. q_j, $\boldsymbol{\mu}_j$, and $\boldsymbol{Q}_j$ are the permanent charge, dipole, and quadrupole on site j, respectively. ξ is the Ewald convergence coefficient that controls the balance between the real and reciprocal space terms in the Ewald computation, and $\boldsymbol{K}$ is a matrix with elements $K_{\alpha\beta} = k_\alpha k_\beta$.

As part of the real space term, the induced dipoles interact with the permanent multipoles via

$$G_{ji}^1(\mathbf{r}_{ji}) = \boldsymbol{\mu}_i^{\text{ind}}\cdot\boldsymbol{\mu}_j + \boldsymbol{\mu}_j^{\text{ind}}\cdot\boldsymbol{\mu}_i + q_j\boldsymbol{\mu}_i^{\text{ind}}\cdot\mathbf{r}_{ji} - q_i\boldsymbol{\mu}_j^{\text{ind}}\cdot\mathbf{r}_{ji}$$

$$G_{ji}^2(\mathbf{r}_{ji}) = -2\boldsymbol{Q}_i:\{\mu_{j,\alpha}^{\text{ind}} r_{ji,\beta}\} - 2\boldsymbol{Q}_j:\{\mu_{i,\alpha}^{\text{ind}} r_{ji,\beta}\}$$

$$G_{ji}^3(\mathbf{r}_{ji}) = \boldsymbol{\mu}_i^{\text{ind}}\cdot\mathbf{r}_{ji}\boldsymbol{Q}_j:\boldsymbol{R}_{ji} - \boldsymbol{\mu}_j^{\text{ind}}\cdot\mathbf{r}_{ji}\boldsymbol{Q}_i:\boldsymbol{R}_{ji} \tag{26}$$

where $\boldsymbol{R}_{ji} = \{r_{ji,\alpha} r_{ji,\beta}\}$, and the colon denotes the scalar product of two matrices, $\boldsymbol{A}:\boldsymbol{B} = \Sigma_\alpha \Sigma_\beta A_{\alpha\beta} B_{\alpha\beta}$.

The screening function in the real space term is given by[46]

$$B_m(r_{ji}) = \frac{(2m)!}{m!2^m r_{ji}^{2m+1}} - \frac{(2\xi^2)^{m+1}}{(2m+1)\xi\sqrt{\pi}} + O_m(r_{ji}) \quad (27)$$

When ξ is set to 0, only the first term of $B_m(r_{ji})$ remains. The real space term then transforms into the standard non-Ewald interaction formula, whereas the reciprocal and self-interaction components disappear. Damping of interactions according to the Thole scheme is achieved by simple application of the damping coefficient, λ, to the screening function

$$B_m'(r_{ji}) = \lambda_{2m+1} \frac{(2m)!}{m!2^m r_{ji}^{2m+1}} \quad (28)$$

The electric field generated by the point multipoles is evaluated from

$$\mathbf{E}_i = -\frac{4\pi}{V}\sum_{\mathbf{k}\neq 0} i\mathbf{k} A_k \sum_j (q_j - i\boldsymbol{\mu}_j\cdot\mathbf{k} - \boldsymbol{Q}_j:\boldsymbol{K}) \exp(-i\mathbf{k}\cdot\mathbf{r}_{ji}) - \sum_{j\neq i}[q_j B_1(r_{ji})\mathbf{r}_{ji} - \boldsymbol{\mu}_j\cdot\mathbf{r}_{ji} B_2(r_{ji})\mathbf{r}_{ji} + B_1(r_{ji})\boldsymbol{\mu}_j + \boldsymbol{Q}_j:\boldsymbol{R}_j B_3(r_{ji})\mathbf{r}_{ji} - B_2(r_{ji})\boldsymbol{Q}_j\cdot\mathbf{r}_{ji}] + \frac{4\xi^3}{3\sqrt{\pi}}\mu_j \quad (29)$$

Similar to above, the three terms correspond to the reciprocal space, real space, and self-interaction components, respectively. To compute the field due only to the induced dipoles, $\boldsymbol{\mu}^{\mathrm{ind}}$ is substituted for $\boldsymbol{\mu}$, and all of the terms involving point charge and quadrupole components disappear.

The Ewald formula for the polarization force at site i is

$$\mathbf{F}_i^{\mathrm{pol}} = -\frac{4\pi}{V}\sum_{k\neq 0} i\mathbf{k} A_k \sum_j [f_{ji}^{\mathrm{ind}} + (\boldsymbol{\mu}_i^{\mathrm{ind}}\cdot\mathbf{k})(\boldsymbol{\mu}_j^{\mathrm{ind}}\cdot k)] \exp(-i\mathbf{k}\cdot\mathbf{r}_{ji}) - \sum_{m=1}^{3}\sum_{j\neq i}[G_{ji}^m(\mathbf{r}_{ji}) B_{m+1}(r_{ji})\mathbf{r}_{ji} + B_m(r_{ji})\nabla_i G_{ji}^m(\mathbf{r}_{ji})] \quad (30)$$

where

$$\nabla_i G_{ji}^1(\mathbf{r}_{ji}) = q_j\boldsymbol{\mu}_j^{\mathrm{ind}} - q_j\boldsymbol{\mu}_i^{\mathrm{ind}}$$

$$\nabla_i G_{ji}^2(\mathbf{r}_{ji}) = 2\boldsymbol{Q}_j\cdot\boldsymbol{\mu}_i^{\mathrm{ind}} - 2\boldsymbol{Q}_i\cdot\boldsymbol{\mu}_j^{\mathrm{ind}} + (\boldsymbol{\mu}_j^{\mathrm{tot}}\cdot\mathbf{r}_{ji})\boldsymbol{\mu}_i^{\mathrm{tot}} + (\boldsymbol{\mu}_i^{\mathrm{tot}}\cdot\mathbf{r}_{ji})\boldsymbol{\mu}_j^{\mathrm{tot}} - (\boldsymbol{\mu}_j\cdot\mathbf{r}_{ji})\boldsymbol{\mu}_i - (\boldsymbol{\mu}_i\cdot\mathbf{r}_{ji})\boldsymbol{\mu}_j$$

$$\nabla_i G_{ji}^3(\mathbf{r}_{ji}) = -2(\boldsymbol{\mu}_i^{\mathrm{ind}}\cdot\mathbf{r}_{ji})\boldsymbol{Q}_j\cdot\mathbf{r}_{ji} + 2(\boldsymbol{\mu}_j^{\mathrm{ind}}\cdot\mathbf{r}_{ji})\boldsymbol{Q}_i\cdot\mathbf{r}_{ji} + (\boldsymbol{Q}_i:\boldsymbol{R}_{ji})\boldsymbol{\mu}_j^{\mathrm{ind}} - (\boldsymbol{Q}_j:\boldsymbol{R}_{ji})\boldsymbol{\mu}_i^{\mathrm{ind}}$$

and $\boldsymbol{\mu}^{\mathrm{tot}} = \boldsymbol{\mu}^{\mathrm{ind}} + \boldsymbol{\mu}$.

The torque due to the interactions between the induced dipole and the field at site i is

$$\mathbf{Tq}_i^{\mathrm{pol}} = \frac{4\pi}{V}\sum_{k\neq 0} A_k \sum_j \mathbf{ft}_{ji}^{\mathrm{ind}} \exp(-i\mathbf{k}\cdot\mathbf{r}_{ji}) + \sum_{m=1}^{3}\sum_{j\neq i} B_m(r_{ji})\mathbf{Gt}_{ji}^m(r_{ji}) + \frac{4\xi^3}{3\sqrt{\pi}}\sum_i (\boldsymbol{\mu}_i\cdot\boldsymbol{\mu}_i^{\mathrm{ind}}) \quad (31)$$

where

$$\mathbf{ft}_{ji}^{\mathrm{ind}} = (q_j - i\mathbf{k}\cdot\boldsymbol{\mu}_j - \boldsymbol{Q}_j:\boldsymbol{K})(i\mathbf{k}\cdot\boldsymbol{\mu}_i^{\mathrm{ind}})$$

$$\mathbf{Gt}_{ji}^1(\mathbf{r}_{ji}) = (q_j\mathbf{r}_{ji} + \boldsymbol{\mu}_j)\cdot\boldsymbol{\mu}_i^{\mathrm{ind}}$$

$$\mathbf{Gt}_{ji}^2(\mathbf{r}_{ji}) = -[(\boldsymbol{\mu}_j\cdot\mathbf{r}_{ji})\mathbf{r}_{ji} + 2(\boldsymbol{Q}\cdot\mathbf{r}_{ji})]\cdot\boldsymbol{\mu}_i^{\mathrm{ind}}$$

$$\mathbf{Gt}_{ji}^3(\mathbf{r}_{ji}) = (\boldsymbol{Q}_j:\boldsymbol{R}_{ji})\mathbf{r}_{ji}\cdot\boldsymbol{\mu}_i^{\mathrm{ind}}$$

Note that the last term of the above equation is the self-interaction between the permanent and induced dipoles on the same site, which has no counterpart in the permanent torque calculation.

To compute pressure, an Ewald formulation of the virial tensor, W, can be derived based on the relation[141]

$$\frac{\partial U}{\partial a_{\alpha\beta}} = \sum_{\gamma=1}^{3} W_{\alpha\gamma} a_{\beta\gamma}^* \quad (32)$$

The real space component of the virial tensor can be computed from[47,48]

$$W_{\alpha\beta}^{\mathrm{real}} = -\sum_{i,j>i} r_{ji,\alpha} F_{ji,\beta}^{\mathrm{real}} \quad (33)$$

where $F_{ji,\beta}^{\mathrm{real}}$ is the Ewald real space force between sites i and j, and the summation is over all pairs of sites. The reciprocal space component is given by

$$W_{\alpha\beta}^{\mathrm{recip}} = \frac{2\pi}{V}\sum_{k\neq 0} A_k |f_{jk}|^2 [2k_\alpha k_\beta (1 + k^2/4\xi^2)/k^2 - \delta_{\alpha\beta}] + \frac{4\pi}{V}\sum_{k\neq 0} A_k \mathscr{R}[\bar{f}_{jk}\sum_j (2k_\alpha \sum_{m=1}^{3} k_m Q_{j,m\beta} + i\boldsymbol{\mu}_{j,\beta}k_\alpha) \exp(-i\mathbf{k}\cdot\mathbf{r}_j)] \quad (34)$$

with $f_{jk} = \Sigma_j(q_j - i\boldsymbol{\mu}_j\cdot\mathbf{k} - \boldsymbol{Q}_j:\boldsymbol{K}) \exp(-i\mathbf{k}\cdot\mathbf{r}_j)$ and $\bar{f}_{jk}$ as the complex conjugate. As with the field computation, the polarization contribution can be obtained by substitution of $\boldsymbol{\mu}^{\mathrm{ind}}$ for $\boldsymbol{\mu}$ in the above equation. The pressure tensor is then computed from the virial tensor and the velocities as

$$P_{\alpha\beta} = \frac{1}{V}[\sum_i m v_{i\alpha} v_{i\beta} - W_{\alpha\beta}] \quad (35)$$

The above formulas apply to a periodic system consisting of an arbitrary number of multipole and polarizable sites. In keeping with traditional molecular mechanics, the short-range intramolecular nonbonded interactions between atoms or sites separated by one, two, or three bonds are usually either omitted or scaled. Meanwhile, in the AMOEBA formulation, the polarization interaction is also damped at very short range. Because almost all of these modifications occur at distances shorter than a typical real space cutoff distance, the most convenient way to proceed is to add to the real space computation $(f_{\mathrm{scale}} - 1)\cdot Y_{AB}$, where f_{scale} is the scaling factor and Y_{AB} is the standard non-Ewald interaction between sites A and B. The value of f_{scale} is 0 for completely omitted interactions, 1 for fully included interactions, and intermediate for scaled interactions. Of course, this scaling procedure must be applied consistently across all energy, force, and electric field calculations.

References and Notes

(1) Burkert, U.; Allinger, N. L. *Molecular Mechanics*; American Chemical Society: Washington DC, 1982.
(2) Bernal, J. D.; Fowler, R. H. *J. Chem. Phys.* **1933**, *1*, 515.
(3) Finney, J. L. *J. Mol. Liq.* **2001**, *90*, 303.

(4) Jorgensen, W. L.; Chandrasekhar, J.; Madura, J. D.; Impey, R. W.; Klein, M. L. *J. Chem. Phys.* **1983**, *79*, 926.
(5) Berendsen, H. J. C.; Postma, J. P. M.; van Gunsteren, W. F.; Hermans, J. Interaction Models for Water in Relation to Protein Hydration. In *Intermolecular Forces*; Pullmann, B., Ed.; D. Reidel Publishing Company: Dordrecht, 1981; p 331.
(6) Mahoney, M. W.; Jorgensen, W. L. *J. Chem. Phys.* **2000**, *112*, 8910.
(7) Berendsen, H. J. C.; Grigera, J. R.; Straatsma, T. P. *J. Phys. Chem.* **1987**, *91*, 6269.
(8) Halgren, T. A.; Damm, W. *Curr. Opin. Struc. Biol.* **2001**, *11*, 236.
(9) Rick, S. W.; Stuart, S. J. *Rev. Comput. Chem.* **2002**, *18*, 89.
(10) Williams, D. E. *J. Comput. Chem.* **1988**, *9*, 745.
(11) Vesely, F. J. *J. Comput. Phys.* **1977**, *24*, 361.
(12) Rappé, A. K.; Goddard, W. A., III. *J. Phys. Chem.* **1991**, *95*, 3358.
(13) Rick, S. W.; Stuart, S. J.; Berne, B. J. *J. Chem. Phys.* **1994**, *101*, 6141.
(14) Stern, H. A.; Rittner, F.; Berne, B. J.; Friesner, R. A. *J. Chem. Phys.* **2001**, *115*, 2237.
(15) Guillot, B.; Guissani, Y. *J. Chem. Phys.* **2001**, *114*, 6720.
(16) Barnes, P.; Finney, J. L.; Nicholas, J. D.; Quinn, J. E. *Nature* **1979**, *282*, 459.
(17) Stillinger, F. H.; David, C. W. *J. Chem. Phys.* **1978**, *69*, 1473.
(18) Matsuoka, O.; Clementi, E.; Yoshimine, M. *J. Chem. Phys.* **1976**, *64*, 1351.
(19) Corongiu, G. *Int. J. Quantum. Chem.* **1992**, *42*, 1209.
(20) Sprik, M.; Klein, M. L. *J. Chem. Phys.* **1988**, *89*, 7556.
(21) Caldwell, J. W.; Kollman, P. A. *J. Phys. Chem.* **1995**, *99*, 6208.
(22) Applequist, J.; Carl, J. R.; Fung, K.-K. *J. Am. Chem. Soc.* **1972**, *94*, 2952.
(23) Bode, K. A.; Applequist, J. *J. Phys. Chem.* **1996**, *100*, 17820.
(24) Bernardo, D. N.; Ding, Y.; Krogh-Jespersen, K.; Levy, R. M. *J. Phys. Chem.* **1994**, *98*, 4180.
(25) Dang, L. X.; Chang, T. M. *J. Chem. Phys.* **1997**, *106*, 8149.
(26) Burnham, C. J.; Li, J. C.; Xantheas, S. S.; Leslie, M. *J. Chem. Phys.* **1999**, *110*, 4566.
(27) Burnham, C. J.; Xantheas, S. S. *J. Chem. Phys.* **2002**, *116*, 1500.
(28) Burnham, C. J.; Xantheas, S. S. *J. Chem. Phys.* **2002**, *116*, 5115.
(29) Buckingham, A. D.; Fowler, P. W. *Can. J. Chem.* **1985**, *63*, 2018.
(30) Dykstra, C. E. *J. Am. Chem. Soc.* **1989**, *111*, 6168.
(31) Dykstra, C. E. *Chem. Rev.* **1993**, *93*, 2339.
(32) Dykstra, C. E. *J. Chem. Phys.* **1989**, *91*, 6472.
(33) Engkvist, O.; Åstrand, P.-O.; Karlström, G. *Chem. Rev.* **2000**, *100*, 4087.
(34) Åstrand, P.-O.; Linse, P.; Karlström, G. *Chem. Phys.* **1995**, *191*, 195.
(35) Brdarski, S.; Åstrand, P.-O.; Karlström, G. *Theor. Chem. Acc.* **2000**, *105*, 7.
(36) Saint-Martin, H.; Hernandez-Cobos, J.; Bernal-Uruchurtu, M. I.; Ortega-Blake, I.; Berendsen, H. J. C. *J. Chem. Phys.* **2000**, *113*, 10899.
(37) Millot, C.; Soetens, J.-C.; Costa, M. T. C. M. *J. Phys. Chem. A* **1998**, *102*, 754.
(38) Keutsch, F. N.; Saykally, R. J. *Proc. Natl. Acad. Sci. U.S.A.* **2001**, *98*, 10533.
(39) Stone, A. J. *The Theory of Intermolecular Forces*; Oxford University Press: Oxford, 1996.
(40) Miller, K. J. *J. Am. Chem. Soc.* **1990**, *112*, 8533.
(41) Stout, J. M.; Dykstra, C. E. *J. Phys. Chem. A* **1998**, *102*, 1576.
(42) Thole, B. T. *Chem. Phys.* **1981**, *59*, 341.
(43) van Duijnen, P. T.; Swart, M. *J. Phys. Chem. A* **1998**, *102*, 2399.
(44) Kong, Y. Multipole Electrostatic Methods for Protein Modeling with Reaction Field Treatment. Ph.D. Thesis, Washington University Medical School, Saint Louis, MO, 1997.
(45) Young, D. M. *Iterative Solution of Large Linear Systems*; Academic Press: New York, 1971.
(46) Smith, W. *CCP5 Newsletter* **1998**, *46*, 18.
(47) Toukmaji, A.; Sagui, C.; Board, J.; Darden, T. *J. Chem. Phys.* **2000**, *113*, 10913.
(48) Nymand, T. M.; Linse, P. *J. Chem. Phys.* **2000**, *112*, 6152.
(49) Tironi, I. G.; Brunne, R. M.; van Gunsteren, W. F. *Chem. Phys. Lett.* **1996**, *250*, 19.
(50) Allinger, N. L.; Yuh, Y. H.; Lii, J.-H. *J. Am. Chem. Soc.* **1989**, *111*, 8551.
(51) Benedict, W. S.; Gailar, N.; Plyler, E. K. *J. Chem. Phys.* **1956**, *24*, 1139.
(52) Dang, L. X.; Pettitt, B. M. *J. Phys. Chem.* **1987**, *91*, 3349.
(53) Halgren, T. A. *J. Am. Chem. Soc.* **1992**, *114*, 7827.
(54) Bagossi, P. unpublished data.
(55) Savage, H. F. J.; Finney, J. L. *Nature* **1986**, *322*, 717.
(56) Hagler, A. T.; Huler, E.; Lifson, S. *J. Am. Chem. Soc.* **1974**, *96*, 5319.
(57) Stewart, R. F.; Davidson, E. R.; Simpson, W. T. *J. Chem. Phys.* **1965**, *42*, 3175.
(58) Coppens, P.; Guru Row, T. N.; Leung, P.; Stevens, E. D.; Becker, P. J.; Yang, Y. W. *Acta. Cryst.* **1979**, *A35*, 63.
(59) Stone, A. J. *Chem. Phys. Lett.* **1981**, *83*, 233.
(60) Frisch, M. J.; Trucks, G. W.; Schlegel, H. B.; Scuseria, G. E.; Robb, M. A.; Cheeseman, J. R.; Zakrzewski, V. G.; Montgomery, J. A., Jr.; Stratmann, R. E.; Burant, J. C.; Dapprich, S.; Millam, J. M.; Daniels, A. D.; Kudin, K. N.; Strain, M. C.; Farkas, O.; Tomasi, J.; Barone, V.; Cossi, M.; Cammi, R.; Mennucci, B.; Pomelli, C.; Adamo, C.; Clifford, S.; Ochterski, J.; Petersson, G. A.; Ayala, P. Y.; Cui, Q.; Morokuma, K.; Malick, D. K.; Rabuck, A. D.; Raghavachari, K.; Foresman, J. B.; Cioslowski, J.; Ortiz, J. V.; Stefanov, B. B.; Liu, G.; Liashenko, A.; Piskorz, P.; Komaromi, I.; Gomperts, R.; Martin, R. L.; Fox, D. J.; Keith, T.; Al-Laham, M. A.; Peng, C. Y.; Nanayakkara, A.; Gonzalez, C.; Challacombe, M.; Gill, P. M. W.; Johnson, B. G.; Chen, W.; Wong, M. W.; Andres, J. L.; Head-Gordon, M.; Replogle, E. S.; Pople, J. A. *Gaussian 98*, revision A.7; Gaussian, Inc.: Pittsburgh, PA, 1998.
(61) Ponder, J. W. *TINKER: Software Tools for Molecular Design*, 3.9 ed.; Washington University School of Medicine: Saint Louis, MO, 2001.
(62) Berendsen, H. J. C.; Postma, J. P. M.; van Gunsteren, W. F.; DiNola, A.; Haak, J. R. *J. Chem. Phys.* **1984**, *81*, 3684.
(63) Helfand, E. *Phys. Rev.* **1960**, *119*, 1.
(64) Gass, D. *J. Chem. Phys.* **1969**, *51*, 4560.
(65) Allen, M. P.; Tildesley, D. J. *Computer Simulation of Liquids*; Oxford University Press: Oxford, 1989.
(66) Lebowitz, J. L.; Percus, J. K.; Verlet, L. *Phys. Rev.* **1967**, *153*, 250.
(67) Cheung, P. S. Y. *Mol. Phys.* **1977**, *33*, 519.
(68) Morishita, T. *J. Chem. Phys.* **2000**, *113*, 2976.
(69) Neumann, M. *Mol. Phys.* **1983**, *50*, 841.
(70) Neumann, M.; Steinhauser, O. *Chem. Phys. Lett.* **1984**, *106*, 563.
(71) Powles, J. G.; Fowler, R. F.; Evans, W. A. B. *Chem. Phys. Lett.* **1984**, *107*, 280.
(72) Simonson, T.; Perahia, D. *Proc. Natl. Acad. Sci. U.S.A.* **1995**, *92*, 1082.
(73) Simonson, T. *Chem. Phys. Lett.* **1996**, *250*, 450.
(74) Wang, L.; Hermans, J. *Mol. Simulat.* **1996**, *17*, 67.
(75) Hayward, J. A.; Reimers, J. R. *J. Chem. Phys.* **1997**, *106*, 1518.
(76) Leadbetter, A. J.; Ward, R. C.; Clark, J. W.; Tucker, P. A.; Matsuo, T.; Suga, H. *J. Chem. Phys.* **1985**, *82*, 424.
(77) Clough, S. A.; Beers, Y.; Klein, G. P.; Rothman, L. S. *J. Chem. Phys.* **1973**, *59*, 2254.
(78) Deutsch, P. W.; Hale, B. N.; Ward, R. C.; Reago, J., D. A. *J. Chem. Phys.* **1983**, *78*, 5103.
(79) Zhu, S. B.; Yao, S.; Zhu, J. B.; Singh, S.; Robinson, G. W. *J. Phys. Chem.* **1991**, *95*, 6211.
(80) Zhu, S. B.; Singh, S.; Robinson, G. W. *J. Chem. Phys.* **1991**, *95*, 2791.
(81) Sciortino, F.; Corongiu, G. *J. Chem. Phys.* **1993**, *98*, 5694.
(82) Levitt, M.; Hirshberg, M.; Sharon, R.; Laidig, K. E.; Daggett, V. *J. Phys. Chem. B* **1997**, *101*, 5051.
(83) Swanton, D. J.; Backsay, G. B.; Hush, N. S. *Chem. Phys.* **1983**, *82*, 303.
(84) Swanton, D. J.; Backsay, G.; Hush, N. S. *J. Chem. Phys.* **1986**, *84*, 5715.
(85) Lie, G. C.; Clementi, E. *Phys. Rev. A* **1986**, *33*, 2679.
(86) Wallqvist, A. *Chem. Phys.* **1990**, *148*, 439.
(87) Whalley, E.; Klug, D. D. *J. Chem. Phys.* **1986**, *84*, 78.
(88) Palmo, K.; Krimm, S. *J. Comput. Chem.* **1998**, *19*, 754.
(89) Dinur, U.; Hagler, A. T. *J. Comput. Chem.* **1995**, *16*, 154.
(90) Cho, K.-H.; Kang, Y. K.; No, K. T.; Scheraga, H. A. *J. Phys. Chem. B* **2001**, *105*, 3624.
(91) Mahoney, M. W.; Jorgensen, W. L. *J. Chem. Phys.* **2001**, *115*, 10758.
(92) Klopper, W.; van Duijneveldt-van de Rijdt, J. G. C. M.; van Duijneveldt, F. B. *Phys. Chem. Chem. Phys.* **2000**, *2*, 2227.
(93) Tschumper, G. S.; Leninger, M. L.; Hoffman, B. C.; Valeev, E. F.; Schaefer, H. F., III.; Quack, M. *J. Chem. Phys.* **2002**, *116*, 690.
(94) Mas, E. M.; Bukowski, R.; Szalewicz, K.; Groenenboom, G. C.; Wormer, P. E. S.; van der Avoird, A. *J. Chem. Phys.* **2000**, *113*, 6687.
(95) *CRC Handbook of Chemistry and Physics*, 82nd ed.; Lide, D. R., Ed.; CRC Press LLC: Boca Raton, FL, 2001.
(96) Kell, G. S.; E., M. G.; Whalley, E. *Proc. R. Soc. London Ser.-A* **1989**, *425*, 49.
(97) Xantheas, S. S.; Burnham, C. J.; Harrison, R. J. **2002**, *116*, 1493.
(98) Lee, H. M.; Suh, S. B.; Lee, J. Y.; Tarakeshwar, P.; Kim, K. S. *J. Chem. Phys.* **2000**, *112*, 9759.
(99) Sorenson, J. M.; Hura, G.; Glaeser, R. M.; Head-Gordon, T. *J. Chem. Phys.* **2000**, *113*, 9149.
(100) Soper, A. K. *Chem. Phys.* **2000**, *258*, 121.
(101) Soper, A. K.; Philips, M. G. *Chem. Phys.* **1986**, *107*, 47.
(102) Silvestrelli, P. L.; Parrinello, M. *J. Chem. Phys.* **1999**, *111*, 3572.
(103) Krynicki, K.; Green, C. D.; Sawyer, D. W. *Faraday Discuss* **1978**, *66*, 199.

(104) Smith, P. E.; van Gunsteren, W. F. *Chem. Phys. Lett.* **1993**, *215*, 315.
(105) Eisenberg, D. S.; Kauzmann, W. *The Structure and Properties of Water*; Oxford University Press: New York, 1969.
(106) Andersen, H. C. *J. Comput. Phys.* **1983**, *52*, 24.
(107) Jorgensen, W. L.; Jenson, C. *J. Comput. Chem.* **1998**, *19*, 1179.
(108) Bertolini, D.; Cassettari, M.; Salvetti, G. *J. Chem. Phys.* **1982**, *76*, 3285.
(109) Sprik, M. *J. Chem. Phys.* **1991**, *95*, 6762.
(110) Coulson, C. A.; Eisenberg, D. *Proc. R. Soc. London Ser.-A* **1966**, *291*, 445.
(111) Silvestrelli, P. L.; Parrinello, M. *Phys. Rev. Lett.* **1999**, *82*, 3308.
(112) Batista, E. R.; Xantheas, S. S.; Jónsson, H. *J. Chem. Phys.* **1999**, *111*, 6011.
(113) Höchtl, P.; Boresch, S.; Bitomsky, W.; Steinhauser, O. *J. Chem. Phys.* **1998**, *109*, 4927.
(114) Ichikawa, K.; Kameda, K.; Yamaguchi, T.; Wakita, H.; Misawa, M. *Mol. Phys.* **1991**, *73*, 79.
(115) Toukan, K.; Rahman, A. *Phys. Rev. B* **1985**, *31*, 2643.
(116) Whalley, E. *J. Chem. Phys.* **1984**, *81*, 4087.
(117) Petrenko, V. F.; Whitworth, R. W. *Physics of Ice*; Oxford University Press: New York, 1999.
(118) Floriano, M. A.; Klug, D. D.; Whalley, E.; Svensson, E. C.; Sears, V. F.; Hallman, E. D. *Nature* **1987**, *329*, 821.
(119) Kuhs, W. F.; Lehmann, M. S. *J. Phys. Chem.* **1983**, *87*, 4312.
(120) Batista, E. R.; Xantheas, S. S.; Jónsson, H. *J. Chem. Phys.* **1998**, *109*, 4546.
(121) Owicki, J. C.; Scheraga, H. A. *J. Am. Chem. Soc.* **1977**, *99*, 7403.
(122) Buch, V.; Sandler, P.; Sadlej, J. *J. Phys. Chem. B* **1998**, *102*, 8641.
(123) Stern, H. A.; Berne, B. J. *J. Chem. Phys.* **2001**, *115*, 7622.
(124) Feynman, R. P. *Statistical Mechanics: A Set of Lectures*; W. A. Benjamin: Reading, MA, 1972.
(125) Wallqvist, A.; Berne, B. J. *Chem. Phys. Lett.* **1985**, *117*, 214.
(126) Lobaugh, J.; Voth, G. A. *J. Chem. Phys.* **1997**, *106*, 2400.
(127) Billeter, S. R.; King, P. M.; van Gunsteren, W. F. *J. Chem. Phys.* **1994**, *100*, 6692.
(128) Partridge, H.; Schwenke, D. W. *J. Chem. Phys.* **1997**, *106*, 4618.
(129) Palmo, K. private communication.
(130) Rick, S. W.; Stuart, S. J.; Bader, J. S.; Berne, B. J. *J. Mol. Liq.* **1995**, *65*−*6*, 31.
(131) Liu, Y. P.; Kim, K.; Berne, B. J.; Friesner, R. A.; Rick, S. W. *J. Chem. Phys.* **1998**, *108*, 4739.
(132) Banks, J. L.; Kaminski, G. A.; Zhou, R. H.; Mainz, D. T.; Berne, B. J.; Friesner, R. A. *J. Chem. Phys.* **1999**, *110*, 741.
(133) Stern, H. A.; Kaminski, G. A.; Banks, J. L.; Zhou, R.; Berne, B. J.; Friesner, R. A. *J. Phys. Chem. B* **1999**, *103*, 4730.
(134) Essmann, U.; Perera, L.; Berkowitz, M. L.; Darden, T.; Lee, H.; Pedersen, L. G. *J. Chem. Phys.* **1995**, *103*, 8577.
(135) Andersen, H. C. *J. Chem. Phys.* **1980**, *72*, 2384.
(136) Nose, S. *Mol. Phys.* **1984**, *52*, 255.
(137) Car, R.; Parrinello, M. *Phys. Rev. Lett.* **1985**, *55*, 2471.
(138) van Belle, D.; Wodak, S. J. *Comput. Phys. Commun.* **1995**, *91*, 253.
(139) Greengard, L.; Rokhlin, V. *J. Comput. Phys.* **1987**, *73*, 325.
(140) Ding, H.-Q.; Karasawa, N.; Goddard, W. A., III. **1992**, *97*, 4309.
(141) Nose, S.; Klein, M. L. *Mol. Phys.* **1983**, *50*, 1055.
(142) Nielsen, I. M. B.; Seidl, E. T.; Janssen, C. L. *J. Chem. Phys.* **1999**, *110*, 9435.
(143) Verhoeven, J.; Dymanus, A. *J. Chem. Phys.* **1970**, *52*, 3222.
(144) Murphy, W. F. *J. Chem. Phys.* **1977**, *67*, 5877.
(145) Maroulis, G. *Chem. Phys. Lett.* **1998**, *289*, 403.
(146) Gregory, J. K.; Clary, D. C.; Liu, K.; Brown, M. G.; Saykally, R. J. *Science* **1997**, *275*, 814.
(147) Curtiss, L. A.; Frurip, D. J.; Blander, M. *J. Chem. Phys.* **1979**, *71*, 2703.
(148) Odutola, J. A.; Dyke, T. R. *J. Chem. Phys.* **1980**, *72*, 5062.
(149) Pugliano, N.; Saykally, R. J. *Science* **1992**, *257*, 1937.
(150) Xantheas, S. S.; Dunning, J. T. H. *J. Chem. Phys.* **1993**, *99*, 8774.
(151) Liu, K.; Brown, M. G.; Saykally, R. J. *J. Phys. Chem. A* **1997**, *101*, 8995.
(152) Kell, G. S. *J. Chem. Eng. Data* **1975**, *20*, 97.
(153) Chen, S.-H.; Toukan, K.; Loong, C.-K.; Price, D. L.; Teixeira, J. *Phys. Rev. Lett.* **1984**, *53*, 1360.
(154) Ricci, M. A.; Nardone, M.; Fontana, A.; Andreani, C.; Hahn, W. *J. Chem. Phys.* **1998**, *108*, 450.
(155) Röttger, K.; Endriss, A.; Ihringer, J. *Acta Cryst.* **1994**, *B50*, 644.
(156) Line, C. M. B.; Whitworth, R. W. *J. Chem. Phys.* **1996**, *104*, 10008.